
Deep Quantile Aggregation

Taesup Kim¹ Rasool Fakoor¹ Jonas Mueller¹ Alexander J. Smola¹ Ryan J. Tibshirani^{1,2}

Abstract

Conditional quantile estimation is a key statistical learning challenge motivated by the need to quantify uncertainty in predictions or to model a diverse population without being overly reductive. As such, many models have been developed for this problem. Adopting a meta viewpoint, we propose a general framework (inspired by neural network optimization) for aggregating any number of conditional quantile models in order to boost predictive accuracy. We consider weighted ensembling strategies of increasing flexibility where the weights may vary over individual models, quantile levels, and feature values. An appeal of our approach is its portability: we ensure that estimated quantiles at adjacent levels do not cross by applying simple transformations through which gradients can be backpropagated, and this allows us to leverage the modern deep learning toolkit for building quantile ensembles. Our experiments confirm that ensembling can lead to big gains in accuracy, even when the constituent models are themselves powerful and flexible.

1. Introduction

Accurately quantifying the uncertainty in predictions is crucial in various high-stakes applications of machine learning, such as finance (Schaumburg, 2012) and healthcare (Palma et al., 2020). To fix ideas, let $Y \in \mathbb{R}$ be a response variable of interest, and let $X \in \mathcal{X}$ denote feature variables we use to predict Y . While uncertainty quantification can certainly be achieved as a byproduct of estimating the conditional distribution of $Y|X = x$, this is often a daunting task, especially in high dimensions (when $\mathcal{X} = \mathbb{R}^d$ and d is large). A simpler and generally more tractable goal is to estimate quantiles of $Y|X = x$ over a discrete set of quantile levels $\mathcal{T} \subseteq [0, 1]$, that is, to estimate

$$g(x; \tau) = F_{Y|X=x}^{-1}(\tau), \quad \tau \in \mathcal{T}, \quad (1)$$

¹Amazon Web Services ²Carnegie Mellon University. Correspondence to: Taesup Kim, Rasool Fakoor, Jonas Mueller <{taesup, fakoor, jonasmue}@amazon.com>.

where for a random variable Z , with cumulative distribution function (CDF) F_Z , we denote its level- τ quantile by $F_Z^{-1}(\tau) = \inf\{z : F_Z(z) \geq \tau\}$. For example, one might choose $\mathcal{T} = \{0.01, \dots, 0.99\}$ to finely characterize the conditional distribution $Y|X = x$. Estimation of conditional quantiles has a rich history in econometrics and statistics, and is widely-used in numerous sciences as a tool for uncertainty quantification, or characterizing heterogeneous outcomes across a diverse population.

In this paper, we consider the task of combining any number of conditional quantile models into a unified model. Done properly, such *model aggregation*, also called *ensembling*, can substantially improve on the accuracy of the individual base models. While this has been well-studied in statistics and machine learning (to be reviewed shortly), aggregating quantile models has received far less attention than aggregating (say) point estimates or densities.

Problem Definition. Assume that we are given a collection of p conditional quantile models $\{\hat{g}_j\}_{j=1}^p$ with respect to a discrete set of m quantile levels \mathcal{T} . Each \hat{g}_j , which we call a *base model*, is an estimate of the true conditional quantile function g in (1). It is convenient to view g and each \hat{g}_j as functions from \mathcal{X} to \mathbb{R}^m , with the components of $g(x)$ denoted $g(x; \tau)$, $\tau \in \mathcal{T}$, and similarly for $\hat{g}_j(x)$. Throughout, we should be careful not to confuse the two dimensions of our estimation problem: we have multiple estimates of the same quantile τ output by the various base models, and on the other “axis”, estimates of multiple quantiles τ_1, \dots, τ_m output by a single base model.

Our goal in this paper is to form an ensemble from the base models,

$$\hat{g} = H(\hat{g}_1, \dots, \hat{g}_p) : \mathcal{X} \rightarrow \mathbb{R}^m.$$

We will mainly focus on linear aggregation procedures H , though we will allow the weights in these linear combinations to be themselves functions of x , as in

$$\hat{g}(x) = \sum_{j=1}^p w_j(x) \cdot \hat{g}_j(x), \quad x \in \mathcal{X}. \quad (2)$$

We will consider different aggregation strategies in which each weight $w_j(x)$ is either a scalar, vector, or matrix (and the product between $w_j(x)$ and $\hat{g}_j(x)$ is to be interpreted accordingly). A standard approach would be to use constant

weights (not functions of x), and to fit these by optimizing (say) the pinball loss of the ensemble over the training data. This problem can be reduced to a linear program (LP), and solved using standard convex optimization packages. Meanwhile, as we will demonstrate in what follows, allowing the weights to depend on x can lead to clear practical benefits, and these weights can be optimized using the power, convenience, and efficiency of modern deep learning toolkits.

A key challenge is to ensure *noncrossing* of estimated quantiles, that is, we must enforce $\hat{g}(x; \tau) \leq \hat{g}(x; \tau')$ whenever $\tau \leq \tau'$. We will introduce simple transformations to guarantee noncrossing that are compatible with backpropagation, and hence these can be seamlessly incorporated into the optimization of ensembles of arbitrary flexibility. Even outside of model aggregation, our backpropagation-friendly noncrossing schemes are quite effective for fitting standalone neural quantile regression models.

Related Work: Quantile Regression. Statistical modeling of quantiles dates back to Galton around 1890, though many facts about quantiles were known long before (Hald, 1998). The modern view on conditional quantile modeling was pioneered by Koenker’s work on *quantile regression* in the 1970s; Koenker (2005) gives an overview. This has remained a topic of great interest, with recent developments in areas like kernel machines (Takeuchi et al., 2006), high-dimensional regression (Belloni & Chernozhukov, 2011), and graphical models (Ali et al., 2016). Important developments in distribution-free calibration using quantile regression are given in Romano et al. (2019); Kivaranovic et al. (2020). The rise of deep learning has spurred new progress on quantile regression with neural networks, e.g., Hatalis et al. (2017); Dabney et al. (2018); Xie & Wen (2019); Tagasovska & Lopez-Paz (2019); Benidis et al. (2020).

Related Work: Model Aggregation. Ensemble methods have a central place in machine learning, with seminal work arising in the 1990s on Bayesian model averaging, bagging, boosting, and stacking; see, e.g., Dietterich (2000) for a review. While the machine learning literature has mostly focused on ensembling point predictions, distributional ensembles have a long tradition in statistics, with a classic reference being Stone (1961). Combining distributional estimates is of particular interest in the forecasting community, see Raftery et al. (2005); Ranjan & Gneiting (2010); Gneiting & Ranjan (2013); Gneiting & Katzfuss (2014); Rasp & Lerch (2018) and references therein. To our knowledge, the majority of work here is focused on aggregating probability densities, and there has been little systematic exploration of how to best aggregate conditional quantile models, especially from a flexible/nonparametric perspective. As perhaps evidence for a dearth of sophisticated aggregation methods, a simple quantile averaging approach won the 2014 Global

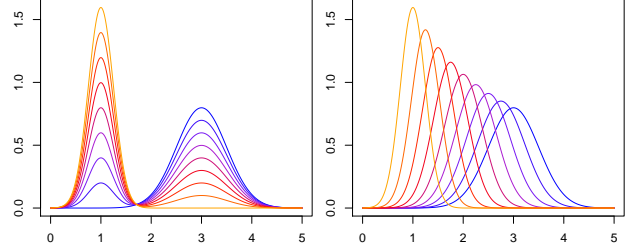


Figure 1: Densities that result from probability averaging (left) or quantile averaging (right) of two normal distributions $N(1, 0.25^2)$ and $N(3, 0.5^2)$, as the weight on the first density varies from 1 (orange) to 0 (blue).

Energy Forecasting Competition (Gaillard et al., 2016). We note that the study of quantile averaging dates back work by to Vincent (a biologist) from the 1910s (Ratcliff, 1979), and some literature thus refers to this method as *Vincentization*.

2. Preliminary Theory

We review some important facts about quantile averaging. For simplicity, we consider marginal quantiles of Y rather than conditional quantiles of $Y|X = x$, but everything covered here can be trivially extended to the conditional setting (simply reinterpret each statement as being conditional on $X = x$). The purpose of this section is to exposit the differences between averaging in the space of quantiles versus probabilities. In this section, when we use the term *average*, we actually refer (more broadly) to a weighted linear combination with weights $w_j \geq 0$ that sum to 1.

For $j = 1, \dots, p$, let F_j be a cumulative distribution function (CDF), let $f_j = F'_j$ be its probability density function, let $Q_j = F_j^{-1}$ denote the corresponding quantile function, and $q_j = Q'_j$ the quantile density function. A standard fact (derived from the chain rule) that relates these objects:

$$q_j(u) = 1/f_j(Q_j(u)) \quad \text{and} \quad f_j(v) = 1/q_j(F_j(v)). \quad (3)$$

Now we consider two ways of averaging distributions. The first way is in probability space, defining $F = \sum_{j=1}^p w_j F_j$. The associated density is simply $f = \sum_{j=1}^p w_j f_j$ (since differentiation is a linear operator). The second way to average is in quantile space, defining $\bar{Q} = \sum_{j=1}^p w_j Q_j$, where now $\bar{q} = \sum_{j=1}^p w_j q_j$ is the associated quantile density (again by linearity of differentiation). Denote the CDF and probability density associated with the quantile average by $\bar{F} = \bar{Q}^{-1}$, and $\bar{f} = \bar{F}'$. Note that, based on (3), we can reason that \bar{f} is a highly nonlinear function of f_j , $j = 1, \dots, p$.

A simple example can go a long way to illustrate the differences between the distributions resulting from probability and quantile averaging. In Figure 1, we compare these two ways applied to a pair of normal distributions with different means and variances. Here we see that probability averaging

produces the familiar mixture of normals, which is bimodal. The result of quantile averaging is extremely different: it is always unimodal, and instead of interpolating between the tail behaviors of f_1 and f_2 (as f does), it appears that *both* tails of f are generally thinner than those of f_1 and f_2 .

It seems that quantile averaging is doing something that is both like translation and scaling in probability density space. The next subsection explains this phenomenon precisely by recalling a classic result. The following subsection recalls another important result on sharpness. The last subsection contributes a small but new result on tail behavior.

2.1. Shape Preservation

An aggregation procedure T is said to be *shape-preserving* provided $F_j \in \mathcal{P}$, $j = 1, \dots, p$, for a location-scale family \mathcal{P} (such as normal, t, Laplace, Cauchy, etc.), implies that $F = T(F_1, \dots, F_p) \in \mathcal{P}$. Probability averaging is clearly not shape-preserving, but quantile averaging is: when each F_j a member of the same location-scale family with some base CDF L , we can write $F_j(v) = L((v - \theta_j)/\sigma_j)$, thus $Q_j(u) = \theta_j + \sigma_j L^{-1}(u)$, so \bar{Q} is still of the form $\theta + \sigma L^{-1}$ and \bar{F} is also in the location-scale family. The next proposition collects this and related results from the literature.

Proposition 1 (Thomas & Ross 1980; Genest 1992)

- (i) Quantile averaging is shape-preserving.
- (ii) Location-scale families \mathcal{P} are the only families with respect to which quantile averaging is a closed operation (meaning $F_j \in \mathcal{P}$, $j = 1, \dots, p$ implies $\bar{F} \in \mathcal{P}$).
- (iii) Quantile averaging is the only aggregation procedure T , among those satisfying (for h not depending on y)

$$T(F_1, \dots, F_p)^{-1}(u) = h(Q_1(u), \dots, Q_p(u)),$$

that is shape-preserving.

Parts (i)-(iii) taken together seem to suggest that quantile averaging is somehow "tailor-made" for shape preservation in a location-scale family. This can be seen as either a pro or a con of quantile averaging, depending on the application one has in mind. To elaborate, let us return for the moment to our regression setting. In an application in which the conditional distribution of $Y|X = x$ is assumed to be (say) normal, and the individual base models each abide by this assumption as they would in (say) Gaussian Process regression, it seems desirable for the ensemble model to retain normality of $Y|X = x$. Quantile averaging would do exactly this. But in an application with no preconceived assumptions on $Y|X = x$, and one in which we are seeking to combine conditional quantile models as a nonparametric mechanism, the shape-preserving quality of quantile averaging would be problematic. For example, a quantile average

of GP regressions would result in a model whose conditionals $Y|X = x$ are still normal. We emphasize that this is very different from probability averaging (as mixtures of normals are a basic building block for nonparametric modeling).

To flexibly model arbitrary conditional distributions without imposing strong assumptions, we are therefore driven to use linear combinations of quantiles which allow different aggregation weights to be used for different quantile levels. But for certain applications (as explained above), it might make sense to limit ourselves to more coarse weights that do not vary over individual quantile levels.

2.2. Moments and Sharpness

Below we recall an important result about moments of the distributions returned by probability and quantile averages. For a distribution G , we denote its uncentered moment of order $k \geq 1$ by $m_k(G) = \mathbb{E}_{X \sim G}(X^k)$.

Proposition 2 (Lichtendahl et al. 2013)

- (i) A probability and quantile average always have equal means, $m_1(F) = m_1(\bar{F})$.
- (ii) A quantile average is always sharper than a probability average, in that $m_k(\bar{F}) \leq m_k(F)$ for any even $k \geq 2$.

Sharpness is only a desirable property if it does not come at the expense of calibration. With this in mind, Proposition 2 cannot be understood as a pro or con of quantile averaging without any context on calibration. That said, the relative sharpness of quantile versus probability averages is an important general fact. Next, we further develop this thread into a more localized view based on the densities.

2.3. Tail Behavior

Here we study the action of quantile averaging on the tails of the subsequent probability density. Simply starting from $\bar{q} = \sum_{j=1}^p w_j q_j$, differentiating, and using (3), yields

$$1/\bar{f}(\bar{Q}(u)) = \sum_{j=1}^p w_j/f_j(Q_j(u)).$$

That is, the probability density \bar{f} at the level- u quantile is a (weighted) *harmonic mean* of the probability densities f_j at their respective level- u quantiles. Since harmonic means are generally (much) smaller than arithmetic means (as we get from probability averaging), we would expect \bar{f} to have thinner tails than f . The next result formalizes this. We use $g(v) = o(h(v))$ to mean $g(v)/h(v) \rightarrow 0$ as $v \rightarrow \infty$, and $g(v) \asymp h(v)$ to mean $g(v)/h(v) \rightarrow c \in (0, \infty)$.

Proposition 3

Assume that $p = 2$, $f_2(v) = o(f_1(v))$, and the weights w_1, w_2 are nontrivial (lying strictly between 0

and 1). Then the density from probability averaging satisfies $f(v) \asymp f_1(v)$. Assuming further that f_1 is log-concave, the density from quantile averaging satisfies $\bar{f}(v) = o(f_1(v))$.

The proof is in Appendix A. The assumption that f_1 is log-concave for the quantile averaging result is stronger than it needs to be (as is the restriction to $p = 2$) but is used to simplify exposition. Proposition 3 reiterates the importance of allowing for level-dependent weights in a linear combination of quantiles. For applications in which there is considerable uncertainty about extreme events (especially ones in which there is disagreement in the degree of uncertainty between individual base models), we would not want an ensemble to de facto inherit a particular tail behavior—whether thin or thick—but want to endow the aggregation procedure with the ability to adapt its tail behavior as needed.

3. Aggregation Methods

In what follows, we introduce various weighted aggregation strategies for combining multiple conditional quantile model into a single unified model. Properly trained, the ensemble should accounting for the strengths/weaknesses of each constituent model, and hence be superior in accuracy to any of the base models. More flexible aggregation strategies can account for finer-grained strengths/weaknesses, provided there is enough data to statistically identify these. We also propose practical optimization algorithms to fit the aggregation weights from data, and introduce techniques to ensure the resulting quantile estimates are noncrossing.

Cross-Validated Ensembling. To avoid overfitting in our ensemble, we utilize a standard cross-validation scheme that only uses out-of-fold predictions from the base models when assigning ensemble weights (Van der Laan et al., 2007; Erickson et al., 2020). Here we randomly partition the training data $\{(x_i, y_i)\}_{i=1}^n$ into K disjoint folds (in our experiments we use $K = 5$). For each data point (x_i, y_i) in a given fold k , we retrain each base model on the other folds $\{1, \dots, K\} \setminus \{k\}$ in order to obtain an out-of-sample prediction at x_i , denoted $\hat{g}_j^{-i}(x_i)$ (the superscript indicates that we have trained on folds that exclude the i th data point). When fitting the ensemble weights, we similarly consider out-of-sample ensemble predictions:

$$\hat{g}(x_i) = \sum_{j=1}^p w_j(x_i) \cdot \hat{g}_j^{-i}(x_i), \quad i = 1, \dots, n. \quad (4)$$

Once the weights have been learned, to make predictions at new test points $x \in \mathcal{X}$, we use (2), where the base models $\{\hat{g}_j\}_{j=1}^p$ have been fit to the full training set $\{(x_i, y_i)\}_{i=1}^n$.

Weighted Ensembling Strategies. Set $w_j(x) = w_j$ for simplicity (the case where the weights depend on x is analo-

gous). We describe weighted ensembling strategies, in order of increasing flexibility (named akin to coffee grind sizes).

- **Coarse:** A single weight w_j is allocated to each base model which is shared over all quantile levels. With p base models, a Coarse aggregator is parameterized by p weights. Each w_j is a scalar, with $\sum_{j=1}^p w_j = 1$. The product “.” in the summands of (2) is interpreted as a scalar-vector product. This is the standard way to build weighted ensembles, but as outlined in Section 2, has clear limitations when done in quantile-space.
- **Medium:** For each quantile level τ , a separate weight w_j^τ is allocated to each base model. With p base models and $m = |\mathcal{T}|$ quantile levels of interest, a Medium aggregator is parameterized by pm weights. Here each w_j is a vector in \mathbb{R}^m , with $\sum_{j=1}^p w_j^\tau = 1$ for each τ . The product “.” in (2) is interpreted as the Hadamard (elementwise) product between vectors. This strategy enables the ensemble to account for the fact that different base models may be better/worse at predicting certain quantile levels, and more generally, as argued in Section 2, enables the ensemble to output models with more flexible tail behavior.
- **Fine:** For each quantile level τ , a separate weight $w_j^{\tau,\nu}$ is allocated to the estimate of a quantile level $\nu \in \mathcal{T}$ output by each base model. With p base models and m quantile levels of interest, a Fine aggregator is parameterized by pm^2 weights. Thus each w_j is actually a matrix in $\mathbb{R}^{m \times m}$, with $\sum_{j=1}^p \sum_{\nu \in \mathcal{T}} w_j^{\tau,\nu} = 1$ for each τ . The product “.” in (2) is interpreted as a matrix-vector product. This strategy presumes that for a given quantile level τ , base model estimates for other levels $\nu \neq \tau$ could be useful for aggregation purposes. Note that this is particularly pertinent to the setting in which some base models are poorly calibrated.

Global versus Local Aggregation. *Global* aggregation weights do not depend on feature values x of the input data. This is how weighted ensembles are traditionally defined. On the other hand *Local* weights refer to a heterogeneous aggregation strategy in which the weights are allowed to vary based on the feature values x . This is akin to a *mixture of experts* approach to ensembling (Jacobs et al., 1991).

To be clear, any combination of Coarse/Medium/Fine and Global/Local can be used for model aggregation (denoted Coarse-Global, Coarse-Local, etc.). Experiments that follow show that the Local-Fine aggregator (the most flexible one), when trained using optimization techniques that are now the standard in deep learning, often performs particularly well. We will subsequently call this Local-Fine aggregator *Deep Quantile Aggregation* (DQA). Next, we detail optimization algorithms to learn ensemble weights in the various setups.

3.1. Global Aggregation via Linear Programming

Given a convex loss function \mathcal{L} acting on quantiles, optimizing the weights with respect to \mathcal{L} for any Global aggregator can be cast as a convex program. We will restrict our attention henceforth to a loss \mathcal{L} defined by summing the *pinball loss* (Koenker & Hallock, 2001) across quantile levels $\tau \in \mathcal{T}$, which simply becomes a linear program (LP).

The pinball loss (also called the tilted- ℓ_1 loss, or quantile score) is defined at a given quantile level τ as

$$l_\tau(y, \hat{y}) = \max\{\tau(y - \hat{y}), (\tau - 1)(y - \hat{y})\}.$$

This piecewise linear function satisfies the following property: for continuous random variable Y , the expected pinball loss $\mathbb{E}[l_\tau(Y, a)]$ is minimized at the level- τ quantile $a = F_Y^{-1}(\tau)$. Our sum of pinball losses remains a *proper scoring rule* for multiple quantile estimates (Gneiting & Raftery, 2007). Given training data $\{(x_i, y_i)\}_{i=1}^n$, we fit ensemble weights by solving the optimization problem

$$\begin{aligned} \text{minimize}_w \quad & \sum_{\tau \in \mathcal{T}} \sum_{i=1}^n l_\tau(y_i, \hat{g}(x_i; \tau)) \\ \text{subject to} \quad & Aw = 1, \quad w \geq 0. \end{aligned} \quad (5)$$

Here $\hat{g}(x_i)$ is the out-of-fold ensemble prediction as in (4), A is a linear operator that encodes the unit-sum constraint:

$$Aw = \begin{cases} \sum_{j=1}^p w_j & \text{for the Coarse case} \\ \sum_{j=1}^p w_j^\tau & \text{for the Medium case} \\ \sum_{j=1}^p \sum_{\nu \in \mathcal{T}} w_j^{\tau, \nu} & \text{for the Fine case,} \end{cases}$$

we use 1 to denote the vector of all 1s, and the constraint $w \geq 0$ is to be interpreted elementwise.

In quantile aggregation, a key challenge is to ensure that the estimates at the multiple quantile levels are in appropriate monotonic order. In the quantile regression literature, this has been addressed by placing constraints on the weights during optimization (as in Takeuchi et al. 2006; Dette & Volgushev 2008; Bondell et al. 2010), or via separate post-processing (as in Chernozhukov et al. 2010; Kuleshov et al. 2018; Song et al. 2019). Following the former strategy, to ensure noncrossing in (5), we can add the following constraints in the optimization problem:

$$\hat{g}(x; \tau) \leq \hat{g}(x; \tau'), \quad \tau < \tau', \quad x \in \mathcal{D}_x, \quad (6)$$

where \mathcal{D}_x is a set of feature values over which we enforce noncrossing. By default we can just use the training feature values $\mathcal{D}_x = \{x_i\}_{i=1}^n$, but we can also additionally include unlabeled points x into \mathcal{D}_x if such test feature values are available at training time. Our experiments use this transductive setting in defining \mathcal{D}_x , highlighting how unlabeled test data can be leveraged in model aggregation. The optimization problem (5), with or without noncrossing constraints

(6), can be reformulated as an LP, which we detail in Appendix B. Functionality for setting up and solving this LP is provided in the `quantgen` R package (Tibshirani, 2020).

The LP formulation, while conceptually tidy, has two limitations: first, it would be difficult to use it for Local aggregation (without adding significant complexity to the optimization formulation); second, even in the current Global setting, solving the LP can be computationally inefficient for large datasets. The developments in the next two subsections are designed to overcome these limitations.

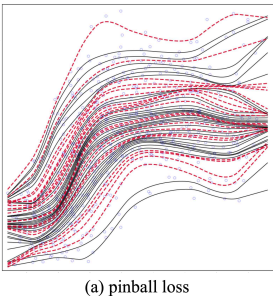
3.2. Aggregation via Gradient-Based Optimization

Instead of solving (5) via linear programming, we propose to apply stochastic gradient descent (SGD) after suitable modifications. SGD algorithms are easily scalable to large datasets (through their use of subsampled mini-batches) and can be implemented via backpropagation in deep learning toolkits that can then leverage hardware accelerators (GPUs). To circumvent the simplex constraints (second line in (5)), we reparametrize the weights in terms of the softmax applied to unconstrained parameters $\{\phi_j\}_{j=1}^p$, as in $w_j = e^{\phi_j} / \sum_{k=1}^p e^{\phi_k}$, $j = 1, \dots, p$ for the case of Coarse weights, and similarly in the other cases. To ensure noncrossing, we adopt a new and efficient strategy described below, that can be viewed as a marriage between optimization-based noncrossing schemes and post-processing ones. We note that, outside of the computational advantages of SGD, the stochastic nature of SGD acts as an implicit regularization mechanism to combat overfitting, and we can further control overfitting by using techniques like early stopping.

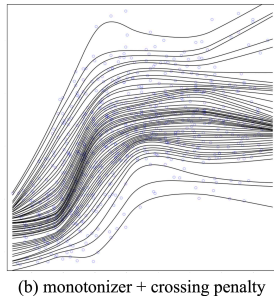
Monotonizer. To replace the noncrossing constraints (6), we propose a *monotonizer* operator that directly fixes crossing quantile estimates in one sweep. For convenience, we index the elements of \mathcal{T} in increasing order, $\tau_1 < \dots < \tau_m$. For a given feature value x and quantile level τ_k , the monotonizer \mathcal{M} applied to \hat{g} returns \tilde{g} defined by

$$\tilde{g}(x; \tau_k) = \begin{cases} \max\{\hat{g}(x; \tau_k), \tilde{g}(x; \tau_{k-1})\} & \tau_k > 0.5 \\ \hat{g}(x; \tau_k) & \tau_k = 0.5 \\ \min\{\hat{g}(x; \tau_k), \tilde{g}(x; \tau_{k+1})\} & \tau_k < 0.5. \end{cases}$$

By construction, this ensures $\tilde{g}(x; \tau) \leq \tilde{g}(x; \tau')$ for $\tau \leq \tau'$. Our monotonizer may be used as a static post-processing layer, or as a dynamic layer used within optimization whose effects are accounted for during learning. For each group of quantile above/below the median, the monotonization transform defined above is sequentially applied in an outwards sweep over the quantile levels in succession. We note that \mathcal{M} can be applied in linear-time, and implemented using the cumulative max/min functions commonly available in deep learning frameworks. Figure 2 shows a simple example of monotonization in action.



(a) pinball loss



(b) monotonizer + crossing penalty

Figure 2: Estimated conditional quantiles across the quantile levels $0.01, 0.03, \dots, 0.99$ from DQR applied to the bone mineral density dataset (with the age feature varying over the x-axis) where DQR optimizes the pinball loss: (a) only, and (b) with the monotonizer and crossing penalty included. Red dashed lines indicate quantile curves that cross others.

Just like the piecewise linear pinball loss, our monotonizer is differentiable almost everywhere, thus when we use it as a layer during optimization, we can backpropagate through it to obtain the necessary gradients for SGD. This is hugely beneficial in practice, as noncrossing can be enforced at basically no extra computational cost. While more sophisticated monotonization operators could be used, like isotonic regression (Barlow et al., 1972), it is unclear how to compute gradients for such operators and this would mean that they could only be applied post-hoc, once the model has been trained. This will typically be worse than learning the weights in an end-to-end fashion that accounts for the effects of monotonization during learning (see Figure 5).

Crossing Penalty. While our monotonizer suffices to ensure noncrossing, it can crudely perturb the original (crossing) aggregated quantile estimates. We additionally introduce a *crossing penalty* during training that smoothly guides the raw estimates to be less nonmonotonic, such that the perturbation from subsequent monotonization is less severe. This leads to more stable optimization and superior estimates (see Figure 5). Our crossing penalty at $x \in \mathcal{X}$ is

$$\rho(\hat{g}(x)) = \sum_{\tau < \tau'} \max\{\hat{g}(x; \tau) - \hat{g}(x; \tau') + \delta, 0\},$$

where the margin $\delta > 0$ is a small constant.

Putting it Together. Incorporating both the monotonizer and crossing penalty, our ultimate objective used to fit aggregation weights via SGD becomes:

$$\sum_{\tau \in \mathcal{T}} \sum_{i=1}^n l_\tau(y_i, \tilde{g}(x_i; \tau)) + \gamma \sum_{x \in \mathcal{D}_x} \rho(\hat{g}(x)). \quad (7)$$

Here we compute the pinball loss of monotonized estimates \tilde{g} . The penalty $\gamma > 0$ can be tuned by cross-validation.

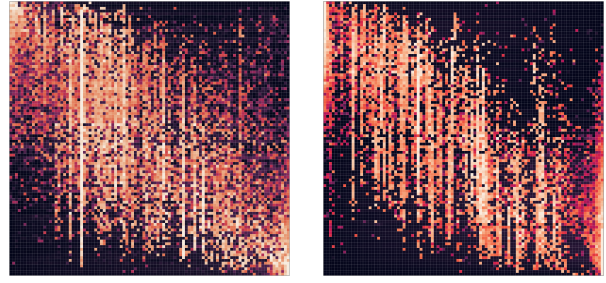


Figure 3: Heatmap of Local-Fine aggregation weights across the concrete (left) and power (right) datasets. For each target quantile level τ (rows), we show weights assigned to base estimates of all quantile levels ν (columns).

3.3. Local Aggregation with Neural Networks

We introduce a Local aggregator, based on a neural network representation, to account for the fact that quantile estimates from the base models may be better/worse at different values of $x \in \mathcal{X}$. For concreteness, we describe this approach for the case of Medium weights, but the same idea applies to Coarse/Fine as well.

To fit weight functions of the form $w_j^\tau : \mathcal{X} \rightarrow \mathbb{R}$, we model these functions jointly (over all base models and quantile levels) using a neural network G . All but the last layer of G forms a feature extractor $f_\theta : \mathcal{X} \rightarrow \mathbb{R}^d$ that maps x into a hidden vector representation $h \in \mathbb{R}^d$. In our experiments, we take f_θ to be a standard feed-forward network parameterized by θ . The last layer of G is defined, for each $\tau \in \mathcal{T}$, by a projection matrix $W^\tau \in \mathbb{R}^{p \times d}$ that maps the hidden representation h , followed by a softmax operation, to local probability weights $w^\tau(x) = (w_1^\tau(x), \dots, w_p^\tau(x))$, as in:

$$w^\tau(x) = G(x; \theta, W^\tau) = \text{softmax}(W^\tau f_\theta(x))$$

The parameters θ and $\{W^\tau\}_{\tau \in \mathcal{T}}$ can be easily optimized via standard SGD methods applied the objective (7) as in the Global setting.

This reflects a *mixture of experts* approach to ensembling (Jacobs et al., 1991). G serves as a gating network that emits predictions from the experts it believes will be most accurate at a particular x . In our most flexible Local-Fine setting (also called DQA), the experts correspond to estimates of individual quantiles from individual base models, and we fit a separate gating scheme for each target quantile level τ . We can also view DQA through the lens of an *attention* mechanism (Bahdanau et al., 2015) that adaptively attends to each quantile from each base model, and uses a different attention map for each target quantile level τ and each x . Visualizing these attention maps (see Figure 3 and Appendix C) helps us interpret for particular quantiles (and particular x): which particular base estimates (and which of their estimated quantiles in Fine settings) are most useful for accurate estimation. Such interpretation is more difficult

Deep Quantile Aggregation

	Model Type	yacht (308)	boston (506)	energy (768)	concrete (1,030)	kin8nm (8,192)	power (9,568)	naval (11,934)	protein (45,730)
Base Models (level 0)	CGN	0.00549	0.08087	0.01714	0.07256	0.07190	0.06235	0.04128	0.18046
	SQR	0.00716	0.08240	0.01522	0.08072	0.07329	0.06319	0.02522	0.16828
	DQR	0.00616	0.07531	0.01385	0.07238	0.06979	0.06119	0.01376	0.15701
	RandomForest	0.01353	0.08797	0.01538	0.08218	0.14889	0.04988	0.01675	0.13222
	ExtraTrees	0.01515	0.08728	0.01538	0.09249	0.15731	0.05461	0.02130	0.14601
	LightGBM	0.00891	0.09679	0.00999	0.06645	0.13943	0.05051	0.02071	0.16083
	LinearRegression	0.13026	0.12437	N/A	0.17752	0.21694	0.07425	N/A	0.23387
	Uniform	0.01989	0.07578	0.01264	0.07511	0.10566	0.05426	0.01744	0.15620
	Global-Coarse	0.00545	0.7452	0.00968	0.05959	0.06813	0.04733	0.01314	0.13213
	Global-Medium	0.00526	0.07488	0.00972	0.05956	0.06821	0.04716	0.01341	0.13211
Quantile Aggregators (level 1)	Global-Medium (LP)	0.00543	0.07555	0.01322	0.06954	0.06814	0.06008	0.01400	N/A
	Global-Fine	0.00580	0.08508	0.00890	0.05761	0.06877	0.04673	0.01329	0.13050
	Local-Coarse	0.00514	0.07582	0.00933	0.05982	0.06812	0.04659	0.01249	0.13127
	Local-Medium	0.00493	0.07610	0.00942	0.06007	0.06815	0.04663	0.01314	0.12924
	Local-Fine	0.00508	0.07537	0.00825	0.05413	0.06839	0.04411	0.01132	0.12533
	Local-Medium (level 1)	0.00587	0.08142	0.01003	0.07061	0.07079	0.04657	0.01349	0.12409
	Local-Fine (level 1)	0.00646	0.08426	0.00959	0.06406	0.07093	0.04622	0.01349	0.12398
	Local-Medium (level 0+1)	0.00532	0.07541	0.00889	0.06109	0.06787	0.04596	0.01145	0.12408
	Local-Fine (level 0+1)	0.00517	0.07521	0.00835	0.05468	0.06783	0.04449	0.01068	0.12389

Table 1: Average pinball loss for UCI datasets (lower is better). Models failing to train in reasonable time were left as N/A. The sample size of each dataset is indicated in parentheses.

for nonlinear quantile stacked ensembles.

3.4. Quantile Aggregation via Stacked Ensembles

While the aforementioned aggregators employ a linear combination of the base predictions, we can also train another (nonlinear) quantile regression model to perform the aggregation instead (Wolpert, 1992). Here we use the same stacked ensembling strategy that Erickson et al. (2020) employed for highly accurate point prediction. We train stacker models (level 1) to operate on features comprised of x and (held out) quantile-predictions from each base model (level 0). As stacker models, we simply try another copy of each of our base models and then use a Local-Medium or Local-Fine weighted ensemble to aggregate (level 1) stacker model quantile estimates. We also try a weighted ensemble that aggregates both stacker and base model estimates (level 0+1). The overall details are provided in Appendix D.

3.5. Deep Quantile Regression Model

We note that the ideas proposed in the previous subsections can be equally-well applied to construct a standalone neural model for multi-quantile regression, which we call Deep Quantile Regression (DQR). Our network simply outputs a vector \mathbb{R}^m to jointly predict all quantile levels in \mathcal{T} and noncrossing is easily enforced by incorporating our monotonizer and crossing penalty from Section 3.2. It is trained using the same objective in (7), again via SGD methods.

4. Experiments

This section studies the empirical performance of our proposed quantile estimation/aggregation procedures. We run several experiments mainly on a set of 8 regression datasets from UCI (Dua & Graff, 2017)¹ that has been established as a popular benchmark in probabilistic deep learning and uncertainty estimation (Mukhoti et al., 2018; Lakshminarayanan et al., 2017; Jain et al., 2020; Fakoor et al., 2020). Appendix I provides similar results over many additional regression datasets from OpenML (Vanschoren et al., 2013). All columns in every dataset (both X and Y) are normalized by their (training split) mean and standard deviation.

Throughout we estimate $\mathcal{T} = \{0.01, 0.02, \dots, 0.99\}$ as our target quantile levels of interest ($m = 99$). Estimating this full spectrum of quantiles is important in applications where we wish to accurately characterize the entire conditional distribution $Y \mid X$, for example, to faithfully model heterogeneous outcomes across a diverse population (Mueller et al., 2018). All experiments are repeated over 5 different random train/test splits and reported results throughout are the average over these replicates.

We obtain multiple quantile estimates $\{\hat{g}_j\}_{j=1}^p$ using $p = 7$ different types of base models. Each base model predicts all quantile levels in \mathcal{T} . We consider three neural network models with different architectures/objectives: (1) conditional Gaussian network (CGN, Lakshminarayanan et al. 2017), (2) simultaneous quantile regression (SQR, Tagasovska & Lopez-Paz 2019), (3) our deep quantile regression (DQR)

¹The *wine* dataset is omitted here, as its Y is discrete ratings.

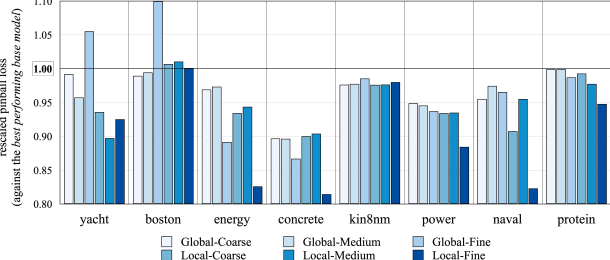


Figure 4: Rescaled pinball loss (lower is better) achieved by various quantile aggregators. Results are scaled against the best performing base model (shown at 1.0 on the y-axis).

model from Section 3.5. We also consider three competitive decision tree variants adapted for quantile regression: (4) random forest (Meinshausen, 2006), (5) extremely randomized trees (Geurts et al., 2006), (6) LightGBM gradient boosting (Ke et al., 2017). Our final base model is standard: (7) linear quantile regression (Koenker et al., 2017). The hyperparameters of every model are tuned via cross-validation over 20 randomly-selected hyperparameter configurations.

All SGD-trained ensemble aggregators incorporate our monotonizer and crossing penalty from Section 3.2. The margin term in our crossing penalty is simply fixed at $\delta = 0.001$ (since all Y have been normalized). Further experiment/model details are provided in Appendix E.

Results. Following Cannon (2018); Gasthaus et al. (2019); Chung et al. (2020); Gneiting & Raftery (2007), we adopt the average pinball loss as a metric to evaluate our quantile estimates. Appendix H additionally reports results in terms of *interval scores*, which evaluate the coverage/sharpness of prediction intervals derived from our quantile estimates (Winkler, 1972). Table 1 and Figure 4 illustrate the performance of each base model and quantile aggregation strategy. While the simplest form of quantile aggregation, a *uniform* (unweighted) average, is not more accurate than best base model on each dataset, Local aggregators outperform not only the base models but also the Global aggregators on all datasets but one. Among Local aggregators, our Local-Fine variant tends to produce the most accurate estimates. This highlights the value of flexible aggregation strategies enabled by our SGD optimization (The LP framework cannot be easily used for Local ensembling).

LP vs. SGD Optimization. Next we use both our SGD method and the straightforward LP formulation to optimize the weights of a Global-Medium quantile aggregator. FICO Xpress Optimization (FICO) is utilized as a LP solver and PyTorch (Paszke et al., 2019) is used to implement our method. Table 1 (compare Global-Medium (LP) vs. Global-Medium) shows that our SGD framework finds superior aggregation weights than the LP approach (see also Appendix B).

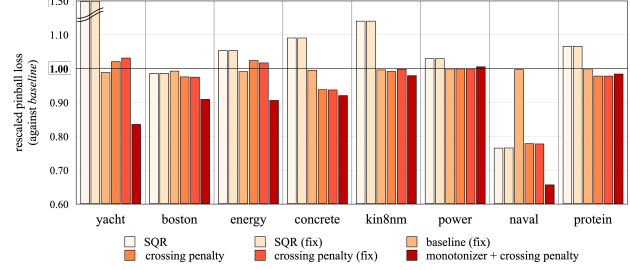


Figure 5: Effect of our monotonizer and crossing penalty on the performance. All pinball losses are scaled so that the *baseline* is as 1.00. In the *fix* settings, the monotonizer is applied post-hoc, but not included in the training objective.

Averaged over 5 runs for the naval dataset, the LP solver takes 61,313 seconds to find an optimal solution, whereas our SGD method converges in only 3,465 seconds (including repeated runs for cross-validation tuning of γ). SGD thus enjoys both a computational advantage over LP optimization of aggregation weights and a statistical advantage (with inherent mechanisms to combat overfitting discussed in Section 3.2 that the LP approach does not possess).

Monotonizer and Crossing Penalty. We examine the effectiveness of our monotonizer and crossing penalty in terms of the deep quantile regression (DQR) neural network from Section 3.5. Here we consider a *baseline* network that shares the same architecture as DQR, but is optimized solely based on the pinball loss (and thus may produce crossing estimates as shown in Figure 2). On top of the baseline, we add only the crossing penalty to see how it improves the performance (*crossing penalty*). We also consider applying the monotonizer post-hoc (after training has completed) to the predictions from the *baseline*, the same model with crossing penalty, as well as an alternative SQR neural quantile regressor proposed by (Tagasovska & Lopez-Paz, 2019) (that does not guarantee noncrossing). Finally we include both the monotonizer and crossing penalty during training as in (7) (*monotonizer + crossing penalty*).

Figure 5 shows the crossing penalty is less effective on its own, and works much better when combined with the monotonizer. These results demonstrate that, beyond avoiding embarrassing estimates, fixing the crossing issue also leads to sizeable accuracy improvements. Post hoc application of the monotonizer (*fix*) is often substantially worse than accounting for its effects during end-to-end training. When trained with both monotonizer and crossing penalty, DQR becomes a powerful model for quantile regression, outperforming the majority of other neural network and tree base models on the majority of datasets (Table 1).

Nonlinear Stacked Ensembling. Table 1 (see also Appendix D) compares the performance of our different stacking strategies from Section 3.4. Straightforward stacked

ensembling (aggregation of level 1 estimates), as successfully employed by Erickson et al. (2020) for point estimates, does not perform better than Local aggregation of the base models. This indicates our adaptive weights already provide sufficient flexibility for accurate quantile aggregation such that the benefits of further nonlinearity are limited. However aggregation of both base (level 0) and stacker (level 1) estimates does often further improve the quantile predictions, particularly for larger datasets. Thus nonlinear stacking is at least valuable for generating additional estimates for our Local aggregator to consider.

References

Ali, A., Kolter, J., and Tibshirani, R. J. The multiple quantile graphical model. In *Advances in Neural Information Processing Systems*, 2016.

Bahdanau, D., Cho, K., and Bengio, Y. Neural machine translation by jointly learning to align and translate. In *International Conference on Learning Representations*, 2015.

Barlow, R., Bartholomew, D., Bremner, J., and Brunk, H. *Statistical Inference Under Order Restrictions: The Theory and Application of Isotonic Regression*. Wiley, 1972.

Belloni, A. and Chernozhukov, V. ℓ_1 -penalized quantile regression in high-dimensional sparse models. *Annals of Statistics*, 39(1):82–130, 2011.

Benidis, K., Rangapuram, S. S., Flunkert, V., Wang, B., Maddix, D., Turkmen, C., Gasthaus, J., Bohlke-Schneider, M., Salinas, D., Stella, L., Callot, L., and Januschowski, T. Neural forecasting: Introduction and literature overview. *arXiv preprint arXiv:2004.10240*, 2020.

Bondell, H. D., Reich, B. J., and Wang, H. Noncrossing quantile regression curve estimation. *Biometrika*, 97(4):825–838, 2010.

Cannon, A. J. Non-crossing nonlinear regression quantiles by monotone composite quantile regression neural network, with application to rainfall extremes. *Stochastic environmental research and risk assessment*, 32(11):3207–3225, 2018.

Chernozhukov, V., Fernández-Val, I., and Galichon, A. Quantile and probability curves without crossing. *Econometrica*, 78(3):1093–1125, 2010.

Chung, Y., Neiswanger, W., Char, I., and Schneider, J. Beyond pinball loss: Quantile methods for calibrated uncertainty quantification. *arXiv preprint arXiv: 2011.09588*, 2020.

Dabney, W., Rowland, M., Bellemare, M., and Munos, R. Distributional reinforcement learning with quantile regression. In *Proceedings of the AAAI Conference on Artificial Intelligence*, 2018.

Dette, H. and Volgushev, S. Non-crossing non-parametric estimates of quantile curves. *Journal of the Royal Statistical Society: Series B*, 70(3):609–627, 2008.

Dietterich, T. G. Ensemble methods in machine learning. In *International workshop on multiple classifier systems*, 2000.

Dua, D. and Graff, C. UCI machine learning repository, 2017. URL <http://archive.ics.uci.edu/ml>.

Erickson, N., Mueller, J., Shirkov, A., Zhang, H., Larroy, P., Li, M., and Smola, A. J. AutoGluon-Tabular: Robust and accurate AutoML for structured data. *arXiv preprint arXiv:2003.06505*, 2020.

Fakoor, R., Mueller, J., Erickson, N., Chaudhari, P., and Smola, A. J. Fast, accurate, and simple models for tabular data via augmented distillation. In *Advances in Neural Information Processing Systems*, 2020.

FICO. Fico xpress optimization suite. URL <http://www.fico.com/en/products/fico-xpress-optimization-suite/>.

Gaillard, P., Goude, Y., and Nedellec, R. Additive models and robust aggregation for GEFCom2014 probabilistic electric load and electricity price forecasting. *International Journal of forecasting*, 32(3):1038–1050, 2016.

Gasthaus, J., Benidis, K., Wang, Y., Rangapuram, S. S., Salinas, D., Flunkert, V., and Januschowski, T. Probabilistic forecasting with spline quantile function RNNs. In *International Conference on Artificial Intelligence and Statistics*, 2019.

Genest, C. Vincentization revisited. *Annals of Statistics*, 20(2):1137–1142, 1992.

Geurts, P., Ernst, D., and Wehenkel, L. Extremely randomized trees. *Machine Learning*, pp. 3–42, 2006.

Gneiting, T. and Katzfuss, M. Probabilistic forecasting. *Annual Review of Statistics and Its Application*, 1:125–151, 2014.

Gneiting, T. and Raftery, A. E. Strictly proper scoring rules, prediction, and estimation. *Journal of the American Statistical Association*, 102(477):359–378, 2007.

Gneiting, T. and Ranjan, R. Combining predictive distributions. *Electronic Journal of Statistics*, 7:1747–1782, 2013.

Hald, A. *A History of Mathematical Statistics from 1750 to 1930*. Wiley, 1998.

Hamill, T. M. and Wilks, D. S. A probabilistic forecast contest and the difficulty in assessing short-range forecast uncertainty. *Weather and Forecasting*, 10(3):620–631, 1995.

Hatalis, K., Lamadrid, A. J., Scheinberg, K., and Kishore, S. Smooth pinball neural network for probabilistic forecasting of wind power. *arXiv preprint arXiv:1710.01720*, 2017.

Jacobs, R. A., Jordan, M. I., Nowlan, S. J., and Hinton, G. E. Adaptive mixtures of local experts. *Neural Computation*, 3:79–87, 1991.

Jain, S., Liu, G., Mueller, J., and Gifford, D. Maximizing overall diversity for improved uncertainty estimates in deep ensembles. In *Proceedings of the AAAI Conference on Artificial Intelligence*, 2020.

Ke, G., Meng, Q., Finley, T., Wang, T., Chen, W., Ma, W., Ye, Q., and Liu, T.-Y. LightGBM: A highly efficient gradient boosting decision tree. In *Advances in Neural Information Processing Systems*, 2017.

Kivaranic, D., Johnson, K. D., and Leeb, H. Adaptive, distribution-free prediction intervals for deep networks. In *International Conference on Artificial Intelligence and Statistics*, 2020.

Koenker, R. *Quantile Regression*. Cambridge University Press, 2005.

Koenker, R. and Hallock, K. F. Quantile regression. *Journal of economic perspectives*, 15(4):143–156, 2001.

Koenker, R., Chernozhukov, V., He, X., and Peng, L. *Handbook of Quantile Regression*. CRC press, 2017.

Kuleshov, V., Fenner, N., and Ermon, S. Accurate uncertainties for deep learning using calibrated regression. In *International Conference on Machine Learning*, 2018.

Lakshminarayanan, B., Pritzel, A., and Blundell, C. Simple and scalable predictive uncertainty estimation using deep ensembles. In *Advances in Neural Information Processing Systems*, 2017.

Lichtendahl, K. C., Grushka-Cockayne, Y., and Winkler, R. L. Is it better to average probabilities or quantiles? *Management Science*, 59(7):1594–1611, 2013.

Meinshausen, N. Quantile regression forests. *Journal of Machine Learning Research*, 7(35):983–999, 2006.

Mueller, J., Jaakkola, T., and Gifford, D. Modeling persistent trends in distributions. *Journal of the American Statistical Association*, 113(523):1296–1310, 2018.

Mukhoti, J., Stenetorp, P., and Gal, Y. On the importance of strong baselines in bayesian deep learning. In *NeurIPS Bayesian Deep Learning Workshop*, 2018.

Palma, M., Tavakoli, S., Brettschneider, J., Nichols, T. E., and Initiative, A. D. N. Quantifying uncertainty in brain-predicted age using scalar-on-image quantile regression. *NeuroImage*, pp. 116938, 2020.

Paszke, A., Gross, S., Massa, F., Lerer, A., Bradbury, J., Chanan, G., Killeen, T., Lin, Z., Gimelshein, N., Antiga, L., Desmaison, A., Kopf, A., Yang, E., DeVito, Z., Raison, M., Tejani, A., Chilamkurthy, S., Steiner, B., Fang, L., Bai, J., and Chintala, S. Pytorch: An imperative style, high-performance deep learning library. In *Advances in Neural Information Processing Systems*. 2019.

Raftery, A. E., Gneiting, T., Balabdaoui, F., and Polakowski, M. Using bayesian model averaging to calibrate forecast ensembles. *Monthly Weather Review*, 133(5):1155–1174, 2005.

Ranjan, R. and Gneiting, T. Combining probability forecasts. *Journal of the Royal Statistical Society: Series B*, 72(1):71–91, 2010.

Rasp, S. and Lerch, S. Neural networks for postprocessing ensemble weather forecasts. *Monthly Weather Review*, 146(11):3885–3900, 2018.

Ratcliff, R. Group reaction time distributions and an analysis of distribution statistics. *Psychological Bulletin*, 86(3):446–461, 1979.

Romano, Y., Patterson, E., and Candès, E. J. Conformalized quantile regression. In *Advances in Neural Information Processing Systems*, 2019.

Schaumburg, J. Predicting extreme value at risk: Nonparametric quantile regression with refinements from extreme value theory. *Computational Statistics & Data Analysis*, 56(12):4081–4096, 2012.

Song, H., Dieth, T., Kull, M., and Flach, P. Distribution calibration for regression. In *International Conference on Machine Learning*, 2019.

Stone, M. The opinion pool. *Annals of Mathematical Statistics*, 32(4):1339–1342, 1961.

Tagasovska, N. and Lopez-Paz, D. Single-model uncertainties for deep learning. In *Advances in Neural Information Processing Systems*, 2019.

Takeuchi, I., Le, Q. V., Sears, T. D., and Smola, A. J. Nonparametric quantile estimation. *Journal of Machine Learning Research*, 7:1231–1264, 2006.

Thomas, E. A. C. and Ross, B. H. On appropriate procedures for combining probability within the same family. *Journal of Mathematical Psychology*, 21:136–152, 1980.

Tibshirani, R. J. quantgen: Tools for generalized quantile modeling, 2020. URL <https://github.com/ryantibs/quantgen>.

Van der Laan, M. J., Polley, E. C., and Hubbard, A. E. Super learner. *Statistical applications in genetics and molecular biology*, 6(1), 2007.

Vanschoren, J., van Rijn, J. N., Bischl, B., and Torgo, L. Openml: Networked science in machine learning. *SIGKDD Explorations*, 15(2):49–60, 2013.

Winkler, R. L. A decision-theoretic approach to interval estimation. *Journal of the American Statistical Association*, 67(337):187–191, 1972.

Wolpert, D. H. Stacked generalization. *Neural networks*, 5(2):241–259, 1992.

Xie, Z. and Wen, H. Composite quantile regression long short-term memory network. In *International Conference on Artificial Neural Networks*, 2019.

Appendix: Deep Quantile Aggregation

A. Proof of Proposition 3.

Proof The result in part (i) of the proposition is immediate from the fact that $f(v) = w_1 f_1(v) + w_2 f_2(v)$ and $f_2(v)/f_1(v) \rightarrow 0$. The result in part (ii) is more subtle. Using (3), note that we may write

$$\frac{1}{\bar{f}(\bar{Q}(u))} = \frac{w_1}{f_1(Q_1(u))} + \frac{w_2}{f_2(Q_2(u))}.$$

Consider

$$\frac{f_1(v)}{\bar{f}(v)} = \frac{w_1 f_1(\bar{Q}(u))}{f_1(Q_1(u))} + \frac{w_2 f_2(\bar{Q}(u))}{f_2(Q_2(u))}.$$

It will be convenient to work on the log scale. Introduce $p_1 = \log f_1$ and $p_2 = \log f_2$. Then it suffices to show that as $u \rightarrow 1$,

$$p_1(\bar{Q}(u)) - p_1(Q_1(u)) \rightarrow \infty, \quad \text{and} \quad p_1(\bar{Q}(u)) - p_2(Q_2(u)) \text{ remains bounded away from } -\infty,$$

or

$$p_1(\bar{Q}(u)) - p_2(Q_2(u)) \rightarrow \infty, \quad \text{and} \quad p_1(\bar{Q}(u)) - p_1(Q_1(u)) \text{ remains bounded away from } -\infty.$$

We now divide the argument into two cases. Without a loss of generality, we set $w_1 = w_2 = 1/2$.

Case 1: $p_1(Q_1(u)) - p_2(Q_2(u))$ **remains bounded away from** $-\infty$. In this case, denoting $v = \bar{Q}(u)$, $v_1 = Q_1(u)$, $v_2 = Q_2(u)$, we have, using log-concavity of p_1 ,

$$\begin{aligned} p_1(v) - p_2(v_2) &= p_1(v_1/2 + v_2/2) - p_2(v_2) \\ &\geq p_1(v_1)/2 + p_1(v_2)/2 - p_2(v_2) \\ &= (p_1(v_1) - p_2(v_2))/2 + (p_1(v_2) - p_2(v_2))/2. \end{aligned}$$

The first term above is bounded below by assumption, and the second term diverges to ∞ (under our hypothesis that $f_2(v)/f_1(v) \rightarrow 0$).

Case 2: $p_1(Q_1(u)) - p_2(Q_2(u)) \rightarrow -\infty$. In this case, we have, just as in the first case,

$$\begin{aligned} p_1(v) - p_1(v_1) &= p_1(v_1/2 + v_2/2) - p_1(v_1) \\ &\geq p_1(v_1)/2 + p_1(v_2)/2 - p_2(v_2) + p_2(v_2) - p_1(v_1) \\ &= -(p_1(v_1) - p_2(v_2))/2 + (p_1(v_2) - p_2(v_2))/2. \end{aligned}$$

Now both terms above diverge to ∞ , and this completes the proof. ■

B. Linear Programming (LP)

Reformulation. Section 3.1 showed that Global aggregation weights can be fit by optimizing (5) with the constraints in (6). Below we formally state the full LP formulation of this optimization (here for our Global-Medium aggregator):

$$\begin{aligned}
 & \underset{w,u}{\text{minimize}} \quad \sum_{\tau \in \mathcal{T}} \sum_{i=1}^n u_i^\tau \\
 & \text{subject to} \quad u_i^\tau \geq \tau \left(y_i - \sum_{j=1}^p w_j^\tau \hat{g}_j(x_i; \tau) \right) \quad \forall (x_i, y_i) \in \mathcal{D}_n \text{ and } \forall \tau \in \mathcal{T}, \\
 & \quad u_i^\tau \geq (\tau - 1) \left(y_i - \sum_{j=1}^p w_j^\tau \hat{g}_j(x_i; \tau) \right) \quad \forall (x_i, y_i) \in \mathcal{D}_n \text{ and } \forall \tau \in \mathcal{T}, \\
 & \quad \sum_{j=1}^m w_j^\tau = 1, w_j^\tau \geq 0 \quad \forall \tau \in \mathcal{T}, \\
 & \quad \sum_{j=1}^p w_j^{\tau_k} \hat{g}_j(x_{i'}; \tau_k) \leq \sum_{j=1}^p w_j^{\tau_{k+1}} \hat{g}_j(x_{i'}; \tau_{k+1}) \quad \forall x_{i'} \in \mathcal{D}_x \text{ and } \forall \tau_k, \tau_{k+1} \in \mathcal{T}
 \end{aligned} \tag{8}$$

Additional Results. Here, we present additional results comparing LP and SGD optimization to fit aggregation weights. Tables S1 and S2 show the performance of Global-Coarse and Global-Medium aggregators fit using these two techniques.

Table S1: Performance of **Global-Coarse aggregator** optimized with LP vs. SGD on the UCI datasets.

	LP		SGD	
	Pinball loss	Interval score	Pinball loss	Interval score
yacht	0.00550	0.18411	0.00545	0.20033
boston	0.07567	1.70976	0.07452	1.72714
energy	0.01328	0.36080	0.00968	0.34259
concrete	0.06989	1.69448	0.05959	1.70450
kin8nm	0.06813	1.71149	0.06813	1.71629
power	0.06034	1.55758	0.04733	1.20494
naval	0.01372	0.48941	0.01314	0.57181

Table S2: Performance of **Global-Medium aggregator** optimized with LP vs. SGD on the UCI datasets.

	LP		SGD	
	Pinball loss	Interval score	Pinball loss	Interval score
yacht	0.00543	0.19259	0.00526	0.15821
boston	0.07555	2.06229	0.07488	1.95853
energy	0.01322	0.37130	0.00972	0.32620
concrete	0.06954	1.84009	0.05956	1.76101
kin8nm	0.06814	1.76113	0.06821	1.76564
power	0.06008	1.59381	0.04716	1.40143
naval	0.01400	0.48300	0.01341	0.45548

C. Visualizing Local Weights

In this section, we study how our quantile aggregation gathers information from the given different base models' different quantile estimates. We focus here on local weights, which are designed to adaptively vary for different $x \in \mathcal{X}$, as described

in Section 3.3. It is of interest to see how the aggregator’s preferences vary between different x . Visually inspecting the weights of our quantile aggregators can thus help us interpret for particular quantiles (and particular x): which particular base estimates (and which of their estimated quantiles in Fine settings) are most useful for accurate estimation.

Local-Medium Aggregator. Here, we inspect the local weights from our Local-Medium aggregator. Figure S1 depicts them as a heatmap visualization. Different heatmaps are generated from different test x , each of size $p \times m$. The columns and rows index different quantile levels τ and base model estimates \hat{g}_j , respectively. It is evident that different x , the aggregator differently weights the base models \hat{g}_j and the weights also vary significantly over different quantile levels τ . Some base models appear to be better than others at estimating certain quantile levels for certain x , while these same models produce less useful estimates for other x, τ .

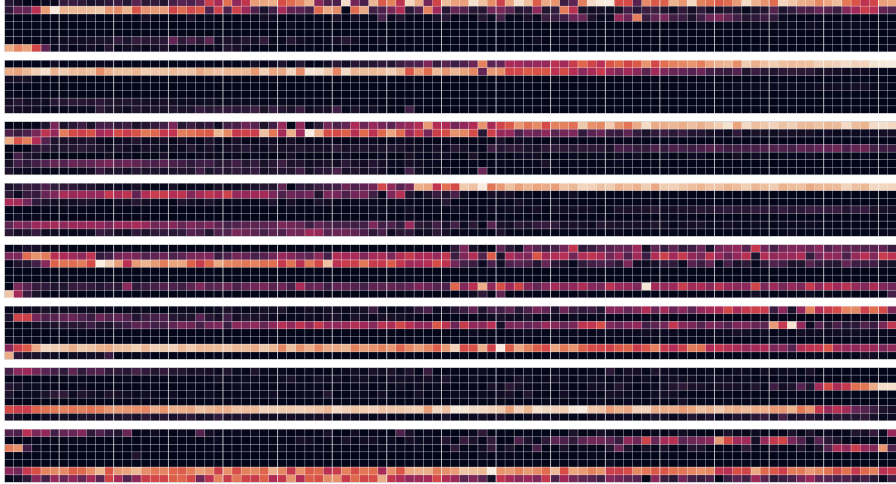


Figure S1: Heatmap visualization of the local weights from the Local-Medium aggregator over the concrete dataset. Each heatmap shows a distinct x and how base models (rows) are locally weighed for each quantile level τ_k (columns).

Local-Fine Aggregator. Our Local-Fine aggregator has the versatility to consider the interaction between different quantiles. Specifically, it learns to adaptively attend to each quantile from each base model and uses a different weight for each target quantile level τ and each x considering their interactions. To get a better understanding of its mechanism, we visualize Local-Fine aggregator weights, where for each x , we now have a large number of weights ($p \times m \times m$). In particular, we are interested in studying how different target/base quantile levels interact with each other during aggregation. We thus average weights across different inputs x in a dataset and across the different base models \hat{g}_j to obtain a single heatmap of size $m \times m$, which only depicts quantile-quantile interactions. Figure 3 shows such a heatmap for each of two different datasets. Here, each row depicts how each target quantile level τ aggregates information across base estimates at different quantile levels ν (columns). Both heatmaps show a common diagonal pattern indicating that the interaction typically occurs between neighboring quantile levels, although the behavior is slightly different in tails (which are presumably harder to estimate).

D. Quantile Aggregation via Stacked Ensembles

Stacked ensembling (Wolpert, 1992; Ting & Witten, 1997) is a powerful form of ensemble learning that often produces the most accurate predictions (Koren, 2009; Erickson et al., 2020). The idea is that a machine learned aggregator may identify how to improve upon certain shortcomings of the base model predictions. In particular, stacking methods based on nonlinear models can additionally exploit interactions between certain base predictions that offer enhanced predictive signal. The nonlinear models can be implemented via any type of quantile regression models, and may thus be even more flexible than the weight-based aggregation discussed in this paper. Here we investigate whether this additional flexibility in the aggregation is beneficial in practice (recalling that more flexible models can produce worse estimates with limited data).

Setting. By using the same stacked ensembling strategy that is employed by [Erickson et al. \(2020\)](#), we define stacker models (level 1) by re-applying our base models such as CGN, SQR, DQR, RandomForest, ExtraTrees, and LightGBM (LinearRegression is omitted as it is a linear model). Each stacker model is trained on a set of features consisting of: the set of predictions from each of original base (level 0) models, concatenated with the original data values x . However, if we use the full set of m quantile estimates from each of p base models, then the inputs to each stacker model have $p \times m$ more dimensions than the original base model inputs. Since $p \times m$ may even exceed the dimensionality of x , such a standard application of stacking suffers from severe *curse of dimensionality*, particularly when m is large. This problem can be alleviated in two ways. The first is: each quantile-level can be independently handled by different stacker model, but this will require more stacker models thus increasing computational costs, and will prevent the stacker from implementing cross-quantile strategies like our Fine aggregation that we have seen perform well. Since our goal here is to investigate increasing the flexibility of the aggregator via stacker, we do not consider this option. Rather we consider a second alternative: we can utilize only a subset of the base quantile estimates for different $\tau \in \mathcal{T}$ by simply subsampling them to reduce the total number of features that we feed to the stacker model. Here we specifically consider taking the estimates only from $\{0.1, 0.5, 0.9\}$ quantile levels ($m' = 3$) (still from each base model) as the additional features for our stacker models. We also briefly experimented with using all quantile-levels in \mathcal{T} as features for the stacker ($m = 99$ for our setting), but preliminary results were extremely poor due to curse of dimensionality. Thus, each stacker model now operates on $m' \times p = 3 \times 7 = 21$ additional features along with original features x . Note that providing the original features to the stacker was shown to be valuable by [Erickson et al. \(2020\)](#). It is especially critical in our setting since the stacker must estimate all quantiles in \mathcal{T} from only estimates for a subset, and thus the stacker must have access to the original x to do this properly.

In contrast, our weighted ensemble quantile aggregators are able to handle this problem by adaptively and flexibly assigning weights to a large number of estimates. Moreover, our weighted ensembling aggregation is computationally far cheaper than training many nonlinear stacker models. Weighted ensembling aggregation is also much more interpretable as the assigned weights explicitly show how the quantile estimates are combined, whereas this is much less clear in a nonlinear black-box stacker model.

Even with stacking, it remains unclear which stacker model should be used. In fact, selecting only a single stacker model is suboptimal as we have seen that basically any set of estimates can be improved via aggregation in practice. Thus, we can simply apply our weighted ensemble quantile aggregators to aggregate estimates from the stacker models (level 1). Or we can apply our weighted aggregation to an even larger set of estimates, namely *both* stacker model and base model estimates (level 0+1; both). The performance of these strategies are summarized in the following table:

Table S3: Performance of quantile aggregation with stacked ensembles.

	Local-Medium			Local-Fine		
	level 0	level 1	both	level 0	level 1	both
yacht	0.0049	0.0059	0.0053	0.0051	0.0065	0.0052
boston	0.0761	0.0814	0.0754	0.0754	0.0843	0.0752
energy	0.0094	0.0100	0.0089	0.0083	0.0096	0.0084
concrete	0.0601	0.0706	0.0611	0.0541	0.0641	0.0547
kin8nm	0.0682	0.0708	0.0679	0.0684	0.0709	0.0678
power	0.0466	0.0466	0.0460	0.0442	0.0462	0.0445
naval	0.0131	0.0135	0.0114	0.0113	0.0135	0.0107
protein	0.1292	0.1241	0.1241	0.1253	0.1240	0.1239

Table S3 clearly shows that stacked ensembling (aggregation of level 1 estimates) does not perform better than Local aggregation of the base models (aggregation of level 0 estimates). This indicates our adaptive weights already provide sufficient flexibility for accurate quantile aggregation such that the benefits of further nonlinearity are limited and may require too much data to be practically useful. However, aggregation of both base and stacker estimates (level 0+1; both) does often further improve the quantile predictions, particularly for larger datasets. Thus, nonlinear stacking is at least valuable for generating additional estimates for our Local aggregator to consider.

E. Experiment and Model Details

Experiment Details All experiments are conducted 5 times by varying the random seed (e.g. seed={1, 2, 3, 4, 5}) which affects the data splits for train/validation/test (0.72 : 0.18 : 0.10), hyper-parameter selection, and model initialization. Reported values throughout are an average over these 5 runs. For base models, we search for the best hyper-parameters via cross-validation over 20 randomly selected hyper-parameter configurations. After the best hyper-parameters are decided, out-of-fold estimates from base models are produced for every training data point via 5-fold ($K = 5$) cross-validation (bagging) by properly re-training base models for each fold. The hyper-parameters for aggregation models are also tuned via cross-validation over 20 randomly-selected hyper-parameter configurations (which with our SGD procedure was still much faster than a single run of the LP optimization).

Base Models. We obtain multiple quantile estimates $\{\hat{g}_j\}_{j=1}^p$ using $p = 7$ different types of base models. Each base model predicts all quantile levels in \mathcal{T} . We first consider three neural network models that compute quantile estimates differently. All models are based on a feed-forward network (multilayer perceptron) and are able to predict all quantile levels from a single network.

- **Conditional Gaussian Network** (CGN, Lakshminarayanan et al. 2017): This model assumes that the conditional distribution $Y|X = x$ is Gaussian. The model therefore outputs estimates of sufficient statistics, namely the conditional mean $\mu(x)$ and variance $\sigma^2(x)$. The model is optimized by minimizing the negative log-likelihood criterion. Subsequent quantile estimation is straightforward that can be computed from $\mathcal{N}(\mu(x), \sigma(x))$ in a closed form (e.g. $\hat{g}(x; \tau) = \mu(x) + \sigma(x)\sqrt{2}\text{erf}^{-1}(2\tau - 1)$).
- **Simultaneous Quantile Regression** (SQR, Tagasovska & Lopez-Paz 2019): This model takes the target quantile level τ as input along with x and then outputs an estimate of the corresponding level- τ quantile. This enables the SQR model to estimate the entire conditional distribution at any quantile (e.g. $\hat{g}(x; \tau) = f(x||\tau)$, where x and τ are concatenated). The model is trained by minimizing a pinball loss for many different randomly sampled quantile levels τ . To estimate multiple quantile-levels with SQR, we must feed in the same input x numerous times, each paired with a different $\tau \in \mathcal{T}$.
- **Deep Quantile Regression** (described in Section 3.5): This model is able to only estimate the pre-defined quantile levels \mathcal{T} , but can simultaneously output all estimates of them (e.g. $\hat{g}(x; \tau_k) = f(x)_k$). This is the only model that uses our monotonizer and crossing penalty as other models cannot directly use it.

All of these models are optimized using Adam (Kingma & Ba, 2015) with mini-batches of size 64. They also all share the same architecture/optimization hyper-parameter search space: # of layers: {2, 3}, # of hidden units: {64, 128}, dropout ratio: {0.0, 0.05, 0.1, 0.2}, learning rate: {1e-3, 5e-4}, weight decay: {1e-5, 5e-7}. In all settings, we use early-stopping where the validation loss is evaluated every epoch and if it has not decreased for the last 50 epochs, the optimization is stopped by returning the epoch with the lowest validation loss.

We also consider other base models, which are not neural networks:

- **RandomForest** (Meinshausen, 2006) and **ExtraTrees** (Geurts et al., 2006): Both models are based on random forests trained as a regular regression task. After training, quantile estimates are computed via a trick based on the empirical quantile estimates. The leaf node of the trees contains many instances of the target value from which one can obtain empirical quantile estimates. We use scikit-garden (<https://scikit-garden.github.io/>) for both models. Both models have the same hyper-parameter search space: # of trees (estimators): {100, 1000} ({100}, for large datasets $n > 10,000$), minimum # of samples for splitting nodes: {4, 8, 16}, minimum # of sample for leaf nodes: {4, 8, 16}
- **LightGBM** (Geurts et al., 2006): LightGBM (<https://lightgbm.readthedocs.io/>) is a gradient boosting framework that uses tree based base learners. As a boosting framework, it can optimize the pinball loss, and thus be directly used for quantile regression. LightGBM handles multiple quantile levels independently by modeling each with a separate model. The hyper-parameter space we use is: # of boosted trees (estimators): {100, 1000} ({100}, for large datasets $n > 10,000$), # of leaves: {10, 50, 100}, minimum child samples: {3, 9, 15}, minimum child weight: {1e-2, 1e-1, 1}, subsample ratio: {0.4, 0.6, 0.8}, subsample ratio of columns: {0.4, 0.6}, L1 regularization weight: {1e-1, 1, 5}, L2 regularization weight: {1e-1, 1, 5}.

- **LinearRegression** (Koenker et al., 2017): LinearRegression is the standard quantile regression model. This approach handles multiple quantile levels independently by fitting separate linear models for each, and we train the model using the default settings in `statsmodels` (<https://www.statsmodels.org>).

Aggregation Models. Aggregation models are designed to linearly combine all estimates from our base models. Here, we explain the details on how the models are designed and optimized.

- **Global Aggregators:** Particularly for the case of Medium weights, each quantile level τ has its own weights and we reparametrize them in terms of the softmax applied to unconstrained parameters $\{\phi_j^\tau\}_{j=1}^p$ as in $w_j^\tau = e^{\phi_j^\tau} / \sum_{k=1}^p e^{\phi_k^\tau}$, $j = 1, \dots, p$. We initialize all parameters $\{\phi_j^\tau\}_{j=1}^p$ by zeros. As the Global aggregators do not require any explicit model (i.e. feedforward network), the hyper-parameter space is only defined by optimization related parameters: learning rate: {1e-3, 5e-4}, weight decay: {1e-5, 1e-7}, crossing penalty weight: {0.1, 0.5, 1.0, 2.0, 5.0}
- **Local Aggregators:** This model requires a network G that outputs the weights as described in Section 3.3. The feature extractor f_θ is a feedforward network and it has hyper-parameters such as the number of layers L and the hidden layer size d . The last layer of G linearly maps the hidden representation $h = f_\theta(x)$, followed by a softmax operation, to local probability weights $w^\tau(x) = (w_1^\tau(x), \dots, w_p^\tau(x))$, where each weight for τ is $w_j^\tau(x) \in \mathbb{R}^p$ for Local-Medium, or $w_j^\tau(x) \in \mathbb{R}^{pm}$ for Local-Fine. This last layer is parametrized, for each $\tau \in \mathcal{T}$, by a projection matrix $W^\tau \in \mathbb{R}^{p \times d}$ in the case of Local-Medium, (or $W^\tau \in \mathbb{R}^{pm \times d}$ for Local-Fine). The hyper-parameter space is defined as: learning rate: {1e-3, 5e-4}, weight decay: {1e-5, 1e-7}, crossing penalty weight: {0.1, 0.5, 1.0, 2.0, 5.0}, # of layers: {2}, # of hidden units: {64, 128}, Dropout ratio: {0.0, 0.05, 0.1, 0.2}.

Both aggregators are optimized by using Adam optimizer (Kingma & Ba, 2015) and the mini-batch size is set as 64 (256, for larger datasets $n > 10,000$). We again employ the same early-stopping strategy previously discussed for our neural network base models.

F. Benefits of Estimating More Quantiles

Here we investigate whether it is beneficial to estimate additional quantiles even if we only care about a specific few. We again consider our previously trained base models that have been fit to predict all 99 quantile levels $\mathcal{T} = \{0.01, 0.02, \dots, 0.99\}$. Now we train two quantile aggregators: one that considers all 99 quantile levels estimated by the base models (i.e. what we have used throughout this paper), and another variant that only considers 19 quantile levels $\mathcal{T}' = \{0.05, 0.10, \dots, 0.95\}$ from the base estimates. Finally, we only measure the performance of the aggregator at quantile levels in \mathcal{T}' , so in theory the aggregator that only sees the base estimates for \mathcal{T}' and tries to predict for \mathcal{T}' should suffice. However Table S4 shows that the aggregators get better as more quantile levels are considered during training. This highlights the regularization benefits of our techniques for enforcing non-crossing, where it may be better to train with more quantiles even if we only care about estimating a specific few. However, our Local-Fine weighting strategy is somewhat less effective when a large number of quantile levels is considered. This is because, it becomes difficult to correctly aggregate all information from a large number of different quantile levels. We expect this can be improved by carefully designing and restricting the aggregation pattern (i.e. allowing aggregation only between neighbored quantile levels)

Table S4: Level- τ pinball loss for each τ shown in the “Quantile” column, produced by an aggregator trained on 99 quantiles, and an aggregator trained with 19 quantiles (specifically the quantiles we are trying to estimate here). These results are for the protein dataset.

Quantile	Local-Coarse		Local-Medium		Local-Fine	
	1%-99% (99 quantiles)	5%-95% (19 quantiles)	1%-99% (99 quantiles)	5%-95% (19 quantiles)	1%-99% (99 quantiles)	5%-95% (19 quantiles)
5%	0.04476	0.04492	0.04335	0.04378	0.04273	0.04265
10%	0.07694	0.07686	0.07471	0.07518	0.07246	0.07174
15%	0.10223	0.10214	0.09976	0.10039	0.09587	0.09406
20%	0.12285	0.12258	0.12038	0.12093	0.11528	0.11144
25%	0.13949	0.13909	0.13695	0.13769	0.13134	0.12634
30%	0.15297	0.15249	0.15048	0.15093	0.14425	0.13831
35%	0.16325	0.16298	0.16156	0.16176	0.15464	0.14803
40%	0.17104	0.17090	0.16988	0.16972	0.16273	0.15531
45%	0.17641	0.17651	0.17591	0.17542	0.16971	0.16068
50%	0.17937	0.17972	0.17870	0.17870	0.17319	0.16470
55%	0.17906	0.17939	0.17658	0.17772	0.17301	0.16425
60%	0.17677	0.17721	0.17419	0.17563	0.17084	0.16150
65%	0.17219	0.17271	0.16951	0.17070	0.16650	0.15659
70%	0.16462	0.16525	0.16184	0.16319	0.15877	0.14916
75%	0.15390	0.15464	0.15108	0.15229	0.14822	0.13873
80%	0.13894	0.13983	0.13654	0.13753	0.13349	0.12530
85%	0.11966	0.12057	0.11743	0.11820	0.11352	0.10799
90%	0.09423	0.09502	0.09212	0.09285	0.08840	0.08599
95%	0.05899	0.05917	0.05716	0.05784	0.05469	0.05403
average	0.13619	0.13642	0.13411	0.13476	0.12998	0.12404

G. Metrics

Below we describe and justify the metrics used for evaluation (on the test data) in our experiments.

Pinball Loss. We calculate the average pinball loss over all quantile levels $\tau \in \mathcal{T}$ ranging from 0.01 to 0.99 in 0.01 increments. Note that this average remains a proper scoring rule for multi-quantile estimates (Gneiting & Raftery, 2007). Not only used as an objective function to guide training, the average pinball loss has been adopted as an appropriate metric to evaluate quantile estimates by Cannon (2018); Gasthaus et al. (2019); Chung et al. (2020).

Interval Score. This score evaluates the quality of prediction intervals (Winkler, 1972), which can naturally be produced from our quantile estimates. The interval score rewards a forecaster for narrow prediction intervals, while giving a penalty (whose size depends on the confidence-level) if an observation falls outside the given prediction interval (Gneiting & Raftery, 2007). Compared to alternative metrics such as expected calibration score, both *sharpness* of the uncertainty estimates and their *coverage* properties are accounted for in the interval score (Gneiting & Raftery, 2007), which has been adopted in sensitive applications by Hamill & Wilks (1995); Chung et al. (2020). It was also used as an optimization objective for quantile models (Chung et al., 2020). We measure the average score over centered prediction intervals ranging from quantile-levels [49%, 51%] to [1%, 99%] in 2% increments (e.g 2%, 4%, ..., 98%).

H. Additional Results for UCI Datasets

In this section, we provide overall results on the UCI datasets (8 datasets). We report the pinball loss and interval score (lower values are better for both metrics), as well as the empirical coverage of the central 90% and 50% prediction intervals (values closer to 90% and 50% are better for these metrics). All metrics are computed on the test data in these tables.

Table S5: Overall results for the UCI datasets (Part I).

	yacht (308)		boston (506)		energy (768)		concrete (1,030)	
	Pinball loss	Interval score	Pinball loss	Interval score	Pinball loss	Interval score	Pinball loss	Interval score
CGN	0.00549	0.14386	0.08087	1.89117	0.01714	0.42368	0.07256	1.64985
SQR	0.00716	0.12396	0.08240	1.59034	0.01522	0.31192	0.08072	1.57220
DQR	0.00616	0.22399	0.07531	1.67686	0.01385	0.40273	0.07238	1.78708
RandomForest	0.01353	0.28773	0.08797	2.59063	0.01538	0.42696	0.08218	2.50894
ExtraTrees	0.01515	0.32914	0.08728	2.81273	0.01538	0.57861	0.09249	3.15178
LightGBM	0.00891	0.65042	0.09679	2.12739	0.00999	0.33479	0.06645	1.99147
LinearRegression	0.13026	1.99935	0.12437	2.82730	N/A	N/A	0.17752	4.10138
Uniform	0.01989	0.46887	0.07578	2.01090	0.01264	0.38962	0.07511	2.19220
Global-Coarse (LP)	0.00550	0.18411	0.07567	1.70976	0.01328	0.36080	0.06989	1.69448
Global-Coarse	0.00545	0.20033	0.07452	1.72714	0.00968	0.34259	0.05959	1.70450
Global-Medium (LP)	0.00543	0.19259	0.07555	2.06229	0.01322	0.37130	0.06954	1.84009
Global-Medium	0.00526	0.15821	0.07488	1.95853	0.00972	0.32620	0.05956	1.76101
Global-Fine	0.00580	0.15175	0.08508	1.51464	0.00890	0.31731	0.05761	1.52328
Local-Coarse	0.00514	0.17697	0.07582	1.75343	0.00933	0.32781	0.05982	1.69648
Local-Medium	0.00493	0.13302	0.07610	1.74402	0.00942	0.28327	0.06007	1.63722
Local-Fine	0.00508	0.12041	0.07537	1.60724	0.00825	0.21999	0.05413	1.39384

Table S6: Overall results for the UCI datasets (Part II).

	kin8nm (8,192)		power (9,568)		naval (11,934)		protein (45,730)	
	Pinball loss	Interval score	Pinball loss	Interval score	Pinball loss	Interval score	Pinball loss	Interval score
CGN	0.07190	1.81872	0.06235	1.66607	0.04128	1.08126	0.18046	4.84186
SQR	0.07329	1.50440	0.06319	1.32014	0.02522	0.61972	0.16828	3.32438
DQR	0.06979	1.85376	0.06119	1.64430	0.01376	0.46928	0.15701	3.61982
RandomForest	0.14889	4.65525	0.04988	1.51362	0.01675	0.84528	0.13222	3.35804
ExtraTrees	0.15731	5.03812	0.05461	1.70923	0.02130	1.19824	0.14601	3.59518
LightGBM	0.13943	3.65442	0.05051	1.16868	0.02071	1.13409	0.16083	3.61974
LinearRegression	0.21694	5.83818	0.07425	1.89121	N/A	N/A	0.23387	4.34796
Uniform	0.10566	3.23390	0.05426	1.49574	0.01744	0.83361	0.15620	3.69877
Global-Coarse (LP)	0.06813	1.71149	0.06034	1.55758	0.01372	0.48941	N/A	N/A
Global-Coarse	0.06813	1.71629	0.04733	1.20494	0.01314	0.57181	0.13213	3.35962
Global-Medium (LP)	0.06814	1.76113	0.06008	1.59381	0.01400	0.48300	N/A	N/A
Global-Medium	0.06821	1.76564	0.04716	1.40143	0.01341	0.45548	0.13211	3.33118
Global-Fine	0.06877	1.70202	0.04673	1.42614	0.01329	0.33642	0.13050	3.24122
Local-Coarse	0.06812	1.71743	0.04659	1.21179	0.01249	0.51100	0.13127	3.32136
Local-Medium	0.06815	1.74869	0.04663	1.37338	0.01314	0.43309	0.12924	3.17276
Local-Fine	0.06839	1.74857	0.04411	1.29783	0.01132	0.21337	0.12533	3.00417

Table S7: The empirical coverage of the central 90% and 50% prediction intervals for UCI datasets (Part I).

		yacht (308)		boston (506)		energy (768)		concrete (1030)	
Central interval		90%	50%	90%	50%	90%	50%	90%	50%
Base model (level 0)	CGN	0.8774	0.5548	0.7804	0.4235	0.8779	0.4883	0.8175	0.4408
	SQR	0.7161	0.4645	0.7686	0.5059	0.7688	0.4883	0.7553	0.4951
	DQR	0.9226	0.7290	0.7882	0.4118	0.8857	0.5299	0.8602	0.4718
	RandomForest	0.8194	0.4194	0.8902	0.5294	0.8312	0.4468	0.9495	0.5981
	ExtraTrees	0.8839	0.4581	0.9725	0.6353	0.8753	0.4649	0.9748	0.6757
	LightGBM	0.4968	0.2387	0.4588	0.2078	0.5377	0.2909	0.4854	0.2583
	LinearRegression	0.8581	0.5097	0.8863	0.4706	N/A	N/A	0.8951	0.4680
	Global-Coarse	0.9548	0.8000	0.8118	0.5294	0.8597	0.5506	0.8233	0.5670
Quantile aggregator (level 1)	Global-Medium	0.9613	0.8194	0.8510	0.5529	0.8961	0.5610	0.8738	0.5942
	Global-Fine	0.7742	0.5161	0.6235	0.3804	0.8805	0.3688	0.8369	0.4214
	Local-Coarse	0.9161	0.6903	0.8000	0.4941	0.8623	0.5610	0.8311	0.5515
	Local-Medium	0.9355	0.7355	0.8471	0.5373	0.9065	0.6104	0.8621	0.6058
	Local-Fine.	0.7935	0.4903	0.7529	0.3490	0.6701	0.3506	0.7806	0.4311

Table S8: The empirical coverage of the central 90% and 50% prediction intervals for UCI datasets (Part II).

		kin8nm (8192)		power (9568)		naval (11934)		protein (45730)	
Central interval		90%	50%	90%	50%	90%	50%	90%	50%
Base model (level 0)	CGN	0.8722	0.4705	0.9097	0.5246	0.8213	0.6677	0.9191	0.5282
	SQR	0.7968	0.5261	0.8339	0.5329	0.9576	0.7233	0.8742	0.5129
	DQR	0.8956	0.4995	0.8888	0.5122	0.9829	0.6951	0.9022	0.5308
	RandomForest	0.9544	0.5707	0.9112	0.5350	0.9511	0.4829	0.9355	0.5793
	ExtraTrees	0.9639	0.6132	0.9331	0.5741	0.9685	0.7980	0.9459	0.6021
	LightGBM	0.6534	0.2907	0.6362	0.3256	0.6255	0.3531	0.8574	0.4669
	LinearRegression	0.8998	0.5029	0.8980	0.5049	N/A	N/A	0.9006	0.5012
	Global-Coarse	0.8895	0.5251	0.8213	0.5365	0.9926	0.8211	0.9425	0.5949
Quantile aggregator (level 1)	Global-Medium	0.9032	0.5288	0.8763	0.5494	0.9933	0.8472	0.9416	0.5969
	Global-Fine	0.9159	0.5288	0.8903	0.4966	0.8328	0.4553	0.8876	0.4866
	Local-Coarse	0.8895	0.5241	0.8297	0.5402	0.9576	0.8077	0.9330	0.5776
	Local-Medium	0.8971	0.5239	0.8803	0.5595	0.9945	0.8946	0.9271	0.5811
	Local-Fine	0.8978	0.5005	0.8617	0.4443	0.6415	0.3251	0.8607	0.4678

I. Additional Results for OpenML Datasets (AutoML Benchmark for Regression)

We present similar results for many additional regression datasets from the OpenML Machine Learning Repository (Vanschoren et al., 2013). In particular, we focus on datasets from the AutoML Benchmark for Regression² (33 datasets), which has been proposed as a diverse collection of datasets representing common types of regression tasks encountered in real-world applications. Some datasets have missing values and non-numerical features, which we resolve by adopting the feature preprocessor from AutoGluon (Erickson et al., 2020). We summarize these datasets in the following table, including the total number of samples, features (after preprocessing) and ratio between them (severity of the curse of dimensionality). Here we omit the ‘boston’ dataset (task id: 4857) as it is already present among our previous UCI datasets. Moreover, the base model ‘Linear Regression’ is discarded as it often fails to converge. All experiments for OpenML datasets are conducted in a similar manner as UCI datasets. To reduce the optimization time, we adaptively vary the mini-batch size by depending on the dataset size (i.e. $2^{3+\lfloor \log_{10} n \rfloor}$) and the early stopping is activated when the validation loss has not decreased for the last 500 updates (i.e. update-steps, not epochs).

Table S9: Description of OpenML datasets (The number of features is obtained after preprocessing.)

Task ID	Dataset name	# of samples (A)	# of features (B)	Ratio (B/A)
359934	tecator	240	124	0.517
4857	boston	506	22	0.043
359931	sensory	576	36	0.063
359947	MIP-2016-regression	1,090	231	0.212
359932	socmob	1,156	39	0.034
167210	Moneyball	1,232	74	0.060
359951	house_prices_nominal	1,460	304	0.208
359945	us_crime	1,994	126	0.063
359930	quake	2,178	3	0.001
359933	space_ga	3,107	6	0.002
359944	abalone	4,177	10	0.002
233215	Mercedes_Benz_Greener_Manufacturing	4,209	894	0.212
359948	SAT11-HAND-runtime-regression	4,440	128	0.029
233214	Santander_transaction_value	4,459	4,971	1.115
13854	QSAR-TID-11	5,742	2,048	0.357
14097	QSAR-TID-10980	5,766	2,048	0.355
359935	wine_quality	6,497	11	0.002
359942	colleges	7,063	438	0.062
359939	topo_2_1	8,885	264	0.030
359940	yprop_4_1	8,885	232	0.026
317612	Brazilian_houses	10,692	52	0.005
359946	pol	15,000	26	0.002
359936	elevators	16,599	18	0.001
359949	house_sales	21,613	92	0.004
359952	house_16H	22,784	16	0.001
359941	OnlineNewsPopularity	39,644	73	0.002
233211	diamonds	53,940	26	0.000
168891	black_friday	166,821	23	0.000
233212	Allstate_Claims_Severity	188,318	898	0.005
317614	Yolanda	400,000	100	0.000
359943	nyc-taxi-green-dec-2016	581,835	233	0.000
233213	Buzzinsocialmedia_Twitter	583,250	84	0.000
359926	Airlines_DepDelay_1M	1,000,000	238	0.000

²<https://www.openml.org/s/269/data>, <https://github.com/openml/automlbenchmark>

Table S10: Overall results for the OpenML datasets (Part I)

	tecator (240)		sensory (576)		MIP-2016... (1,090)		socmob (1,156)	
	Pinball loss	Interval score	Pinball loss	Interval score	Pinball loss	Interval score	Pinball loss	Interval score
CGN	0.01730	0.60626	0.23603	5.74099	0.01871	0.55271	0.02678	0.68596
SQR	0.01392	0.24516	0.23542	4.94355	0.00910	0.17242	0.03341	0.58981
DQR	0.01479	0.36195	0.23221	5.78900	0.00857	0.24073	0.03143	0.83488
RandomForest	0.03316	1.04753	0.21730	6.04399	0.00603	0.09951	0.05792	1.14193
ExtraTrees	0.04819	1.78851	0.21726	6.04699	0.00649	0.10590	0.04926	1.18476
LightGBM	0.03529	1.86125	0.23227	4.90567	0.01292	1.20558	0.04063	0.96625
Uniform	0.02117	0.93054	0.22092	5.46045	0.00846	0.37345	0.03117	0.81887
Global-Coarse	0.01327	0.37004	0.21731	6.04543	0.00647	0.10632	0.02643	0.70882
Global-Medium	0.01321	0.34762	0.21684	6.02921	0.00641	0.11045	0.02713	0.76697
Global-Fine	0.01303	0.31732	0.22678	6.06806	0.00706	0.14634	0.02903	0.70326
Local-Coarse	0.01434	0.37090	0.21738	5.89436	0.00618	0.10913	0.02730	0.67986
Local-Medium	0.01340	0.34561	0.21716	5.76543	0.00602	0.11168	0.02821	0.67401
Local-Fine	0.01248	0.30097	0.26346	6.14034	0.00657	0.10850	0.03642	0.69034

Table S11: Overall results for the OpenML datasets (Part II)

	Moneyball (1,232)		house_prices... (1,460)		us_crime (1,994)		quake (2,178)	
	Pinball loss	Interval score	Pinball loss	Interval score	Pinball loss	Interval score	Pinball loss	Interval score
CGN	0.06662	1.78899	0.06196	1.60929	0.13962	3.51845	0.26515	7.15684
SQR	0.06607	1.42013	0.06355	1.16055	0.13675	2.41907	0.25827	4.55538
DQR	0.06515	1.79578	0.05849	2.19753	0.12707	2.89243	0.25160	4.59517
RandomForest	0.07327	2.11786	0.08488	2.65895	0.13036	2.76111	0.25391	4.23138
ExtraTrees	0.07477	2.61312	0.08816	2.89817	0.13268	2.82632	0.24992	4.19011
LightGBM	0.07149	2.30510	0.07493	2.33179	0.13534	2.91532	0.26297	4.34941
Uniform	0.06306	1.92292	0.06036	1.99985	0.12529	2.76994	0.25366	4.78059
Global-Coarse	0.06365	1.69852	0.05688	1.83943	0.12508	2.76957	0.25045	4.24956
Global-Medium	0.06350	1.78562	0.05724	2.04361	0.12503	2.70742	0.25045	4.20714
Global-Fine	0.06332	1.72811	0.05709	1.97296	0.12378	2.60432	0.25106	4.36652
Local-Coarse	0.06342	1.71505	0.05751	1.80772	0.12553	2.72144	0.25033	4.23157
Local-Medium	0.06309	1.75556	0.05717	1.92160	0.12621	2.64598	0.25030	4.19434
Local-Fine	0.06503	1.77440	0.05567	1.81055	0.12463	2.64291	0.24985	4.19546

Table S12: Overall results for the OpenML datasets (Part III).

	space_ga (3,107)		abalone (4,177)		Mercedes... (4,209)		SAT11-HAND... (4,440)	
	Pinball loss	Interval score	Pinball loss	Interval score	Pinball loss	Interval score	Pinball loss	Interval score
CGN	0.12170	3.07323	0.17145	4.53343	0.18209	4.70192	0.13862	4.16538
SQR	0.13511	2.85751	0.17415	3.25710	0.15741	3.07721	0.08736	1.87056
DQR	0.12549	3.40839	0.16997	3.73084	0.15448	3.02610	0.07370	2.41047
RandomForest	0.13936	4.80329	0.17308	3.65737	0.15131	2.98293	0.08216	2.58421
ExtraTrees	0.14771	5.38469	0.17074	3.72229	0.15146	2.96895	0.08517	2.76907
LightGBM	0.14007	3.41344	0.18148	3.71307	0.15406	2.88616	0.09670	3.89518
Uniform	0.12455	3.67388	0.16890	3.68892	0.15166	3.16755	0.08822	2.86382
Global-Coarse	0.12191	3.48209	0.16892	3.72230	0.14999	2.96646	0.08454	2.73831
Global-Medium	0.12161	3.73004	0.16883	3.72281	0.14951	2.99124	0.08268	2.74154
Global-Fine	0.12278	3.73127	0.16990	3.71794	0.14970	3.06551	0.08749	2.72385
Local-Coarse	0.12525	3.43228	0.16829	3.81402	0.15000	2.95241	0.08537	2.47117
Local-Medium	0.12459	3.59119	0.16824	3.71174	0.14962	2.96132	0.07997	2.57845
Local-Fine	0.12352	3.49050	0.16908	3.76958	0.14901	2.89008	0.07604	2.41874

Table S13: Overall results for the OpenML datasets (Part IV)

	Santander... (4,459)		QSAR-TID-11 (5,742)		QSAR-TID-10... (5,766)		wine_quality (6,497)	
	Pinball loss	Interval score	Pinball loss	Interval score	Pinball loss	Interval score	Pinball loss	Interval score
CGN	0.26499	7.27608	0.25036	4.92411	0.29503	5.55254	0.21747	5.46366
SQR	0.33786	6.08938	0.25076	4.37962	0.29201	5.13215	0.21732	4.12475
DQR	0.24877	4.42004	0.24066	4.79227	0.28322	5.58554	0.20457	5.54458
RandomForest	0.21215	3.66346	0.24035	5.59485	0.25680	5.71998	0.17508	5.24544
ExtraTrees	0.21346	3.68614	0.24038	5.59629	0.25684	5.72005	0.18290	5.63563
LightGBM	0.21947	3.78189	0.22383	5.48451	0.25592	5.24258	0.19109	4.18764
Uniform	0.22531	4.28097	0.22051	4.75042	0.25737	5.15645	0.19470	4.96633
Global-Coarse	0.21052	3.64622	0.22093	4.84248	0.24899	5.30154	0.18319	5.62421
Global-Medium	0.21077	3.65495	0.21044	5.21325	0.24574	5.63984	0.18299	5.51258
Global-Fine	0.21144	3.67695	0.20807	5.29747	0.24254	5.62638	0.18406	5.27690
Local-Coarse	0.21220	3.66806	0.23448	4.76457	0.25994	5.51817	0.18215	5.54895
Local-Medium	0.21164	3.66691	0.23418	5.02972	0.26142	5.63281	0.18205	5.20105
Local-Fine	0.21071	3.65324	0.23716	4.82746	0.27973	5.58813	0.17958	4.77847

Table S14: Overall results for the OpenML datasets (Part V).

	colleges (7,063)		topo_2_1 (8,885)		yprop_4_1 (8,885)		Brazilian... (10,692)	
	Pinball loss	Interval score	Pinball loss	Interval score	Pinball loss	Interval score	Pinball loss	Interval score
CGN	0.18643	4.49081	0.23078	6.49501	0.23662	6.59867	0.01270	0.29320
SQR	0.18917	3.66547	0.23357	4.24451	0.23962	4.21457	0.01151	0.21519
DQR	0.18502	4.86582	0.22189	5.35600	0.22326	5.21661	0.01090	0.21761
RandomForest	0.17482	5.14165	0.22328	5.54635	0.21690	5.36174	0.01369	0.31154
ExtraTrees	0.17531	5.25226	0.22118	5.53266	0.21775	5.51919	0.01427	0.41755
LightGBM	0.16982	4.14788	0.22699	4.60117	0.22113	4.56452	0.01332	0.54649
Uniform	0.17110	4.44301	0.22055	5.20049	0.21851	5.11509	0.01178	0.32513
Global-Coarse	0.16767	4.38451	0.22044	5.43679	0.21645	5.31192	0.01077	0.22577
Global-Medium	0.16717	4.91031	0.22032	5.50646	0.21647	5.47380	0.01088	0.23126
Global-Fine	0.16656	4.85382	0.22061	5.46630	0.21696	5.45375	0.01109	0.20131
Local-Coarse	0.16881	4.50781	0.22154	5.38268	0.21793	5.35679	0.01073	0.22176
Local-Medium	0.16845	4.73198	0.22185	5.54414	0.21747	5.48591	0.01055	0.21762
Local-Fine	0.16528	4.71470	0.22138	5.59386	0.21747	5.51070	0.01024	0.19463

Table S15: Overall results for the OpenML datasets (Part VI).

	pol (15,000)		elevators (16,599)		house_sales (21,613)		house_16H (22,784)	
	Pinball loss	Interval score	Pinball loss	Interval score	Pinball loss	Interval score	Pinball loss	Interval score
CGN	0.10245	3.10006	0.07802	2.12042	0.06479	1.72011	0.10519	2.75193
SQR	0.03246	0.65211	0.08110	1.62929	0.06631	1.26507	0.10260	1.86323
DQR	0.02692	0.85809	0.07620	1.91870	0.06441	1.59591	0.09701	2.09633
RandomForest	0.01342	0.43206	0.10182	2.61907	0.06816	1.81827	0.09831	2.10331
ExtraTrees	0.02392	1.27186	0.10730	2.87942	0.06940	1.98718	0.10583	2.26631
LightGBM	0.06030	2.22929	0.09376	2.51618	0.06335	1.75894	0.10271	2.16508
Uniform	0.03731	1.36443	0.08186	2.19362	0.06104	1.62969	0.09562	2.12651
Global-Coarse	0.01357	0.43884	0.07555	1.92151	0.06018	1.61857	0.09381	2.10712
Global-Medium	0.01366	0.44777	0.07550	1.92442	0.06008	1.56052	0.09388	1.97745
Global-Fine	0.01315	0.34767	0.07552	1.84549	0.05974	1.51752	0.09478	1.97636
Local-Coarse	0.01347	0.44204	0.07542	1.88994	0.05956	1.60397	0.09359	2.06361
Local-Medium	0.01347	0.43700	0.07502	1.87468	0.05948	1.55997	0.09357	1.95391
Local-Fine	0.01246	0.34402	0.07400	1.85895	0.05820	1.53697	0.09287	1.91747

Table S16: Overall results for the OpenML datasets (Part VII).

	OnlineNews...		diamonds		black_friday		Allstate_Claims...	
	Pinball loss	Interval score	Pinball loss	Interval score	Pinball loss	Interval score	Pinball loss	Interval score
CGN	0.13789	4.99023	0.03011	0.81621	0.20291	5.32027	0.14824	4.03065
SQR	0.09378	1.61469	0.03070	0.64339	0.21186	4.78521	0.14715	2.72813
DQR	0.09226	1.64630	0.02921	0.87022	0.19246	5.18581	0.14288	3.03738
RandomForest	0.09266	1.63934	0.02417	0.70889	0.18012	4.86993	0.14808	3.13378
ExtraTrees	0.09226	1.63697	0.02423	0.79104	0.17977	4.88650	0.14815	3.14134
LightGBM	0.09253	1.61329	0.02438	1.03722	0.18246	4.97312	0.14296	3.05522
Uniform	0.09590	2.13792	0.02461	0.78450	0.18727	4.95790	0.14207	3.13355
Global-Coarse	0.09180	1.62472	0.03011	0.81620	0.17971	4.88659	0.14117	3.01641
Global-Medium	0.09167	1.61506	0.02934	0.83836	0.17970	4.92093	0.14117	3.03709
Global-Fine	0.09222	1.74977	0.03560	0.87273	0.17985	4.86946	0.14179	2.99423
Local-Coarse	0.09189	1.62241	0.02866	0.81500	0.17977	4.88809	0.14119	3.03499
Local-Medium	0.09177	1.60795	0.02841	0.79985	0.17963	4.92543	0.14112	3.03986
Local-Fine	0.09165	1.60649	0.03796	0.82953	0.17960	4.94477	0.14065	3.02716

Table S17: Overall results for the OpenML datasets (Part VIII).

	Yolanda (400,000)		nyc-taxi...		Buzzinsocial...		Airlines_Dep...	
	Pinball loss	Interval score	Pinball loss	Interval score	Pinball loss	Interval score	Pinball loss	Interval score
CGN	0.19873	5.30382	0.11511	3.14641	0.03712	1.14424	0.20528	6.74235
SQR	0.19761	4.66416	0.11651	2.88898	0.03051	0.58833	0.16083	2.80049
DQR	0.18922	6.19158	0.09883	2.80689	0.02947	0.77558	0.15904	2.94794
LightGBM	0.19972	6.60044	0.08982	2.49865	0.02432	0.69130	0.15681	2.88334
Uniform	0.19159	5.60777	0.09970	2.77262	0.02784	0.76867	0.16446	3.77202
Global-Coarse	0.18902	6.03730	0.08897	2.53835	0.02461	0.69350	0.15680	2.89355
Global-Medium	0.18900	6.10560	0.08847	2.52395	0.02465	0.65747	0.15691	2.93301
Global-Fine	0.18919	6.02834	0.08721	2.32261	0.02464	0.67128	0.15709	3.02797
Local-Coarse	0.18894	6.06081	0.08771	2.52869	0.02454	0.68553	0.15685	2.88597
Local-Medium	0.18890	6.06189	0.08678	2.52808	0.02459	0.65483	0.15694	2.92375
Local-Fine	0.18878	6.00659	0.07580	2.11214	0.02382	0.62319	0.15662	2.92048

(Both RandomForest and ExtraTrees models failed to fit these datasets in reasonable time.)

Additional References for the Appendix

Cannon, A. J. Non-crossing nonlinear regression quantiles by monotone composite quantile regression neural network, with application to rainfall extremes. *Stochastic environmental research and risk assessment*, 32(11):3207–3225, 2018.

Chung, Y., Neiswanger, W., Char, I., and Schneider, J. Beyond pinball loss: Quantile methods for calibrated uncertainty quantification. *arXiv preprint arXiv: 2011.09588*, 2020.

Erickson, N., Mueller, J., Shirkov, A., Zhang, H., Larroy, P., Li, M., and Smola, A. J. AutoGluon-Tabular: Robust and accurate AutoML for structured data. *arXiv preprint arXiv:2003.06505*, 2020.

Gasthaus, J., Benidis, K., Wang, Y., Rangapuram, S. S., Salinas, D., Flunkert, V., and Januschowski, T. Probabilistic forecasting with spline quantile function RNNs. In *International Conference on Artificial Intelligence and Statistics*, 2019.

Geurts, P., Ernst, D., and Wehenkel, L. Extremely randomized trees. *Machine Learning*, pp. 3–42, 2006.

Gneiting, T. and Raftery, A. E. Strictly proper scoring rules, prediction, and estimation. *Journal of the American Statistical Association*, 102(477):359–378, 2007.

Kingma, D. P. and Ba, J. Adam: A method for stochastic optimization. 2015. International Conference for Learning Representations.

Koenker, R., Chernozhukov, V., He, X., and Peng, L. *Handbook of Quantile Regression*. CRC press, 2017.

Koren, Y. The Bellkor solution to the Netflix grand prize. 2009.

Lakshminarayanan, B., Pritzel, A., and Blundell, C. Simple and scalable predictive uncertainty estimation using deep ensembles. In *Advances in Neural Information Processing Systems*, 2017.

Meinshausen, N. Quantile regression forests. *Journal of Machine Learning Research*, 7(35):983–999, 2006.

Tagasovska, N. and Lopez-Paz, D. Single-model uncertainties for deep learning. In *Advances in Neural Information Processing Systems*, 2019.

Ting, K. M. and Witten, I. H. Stacking bagged and dagged models. In *International Conference on Machine Learning*, 1997.

Vanschoren, J., van Rijn, J. N., Bischl, B., and Torgo, L. Openml: Networked science in machine learning. *SIGKDD Explorations*, 15(2):49–60, 2013.

Winkler, R. L. A decision-theoretic approach to interval estimation. *Journal of the American Statistical Association*, 67 (337):187–191, 1972.

Wolpert, D. H. Stacked generalization. *Neural networks*, 5(2):241–259, 1992.